

Overlapping roles of *Iroquois* Homeobox Genes 3 and 4 in the Compaction of the Ventricular Myocardium

by

Wei Fan Liu

A thesis submitted in conformity with the requirements
for the degree of Master of Science

Department of Molecular Genetics
University of Toronto

© Copyright by Wei Fan Liu 2017

Overlapping Roles of *Iroquois* Homeobox Genes 3 and 4 in the Compaction of the Ventricular Myocardium

Wei Fan Liu

Master of Science

Department of Molecular Genetics
University of Toronto

2017

Abstract

Left ventricular noncompaction (LVNC) is a primary congenital cardiomyopathy characterized by prominent trabeculation and intra-trabecular recesses in the ventricular wall. Its genetic basis and pathologic mechanism remain largely unknown. Here it is shown that *Irx3;Irx4* double knockout (DKO) mouse mutants represent a novel model of LVNC. *Irx3* and *Irx4* belong to the family of *Iroquois* homeobox (*Irx*) genes, encoding transcription factors important for cardiac function. Mice lacking either *Irx3* or *Irx4* do not have gross cardiac malformations. In contrast, *Irx3;Irx4*DKO mice exhibit postnatal lethality and thinner ventricular walls as early as E14.5. By P14, DKO mice have prominent noncompacted trabeculation and abnormal muscular growth that resemble human LVNC. Furthermore, *Irx3;Irx4*DKO hearts exhibit increased expression of heart failure marker genes, elevated Bmp10 pathway activity, and altered pattern of cardiomyocyte proliferation, each of which are implicated in the pathogenesis of LVNC. Taken together, these studies suggest that *Irx3* and *Irx4* possess overlapping functions, which are essential to myocardial compaction.

Acknowledgments

I would like to thank my supervisor Dr. C-c Hui for his guidance and support throughout my studies and everyone in the Hui lab for their contributions scientifically and intellectually, especially Dr. Kyoung-Han Kim who performed echocardiography and Rong Mo who assisted in the analysis of *Irx4*KO mice. As well, I am very grateful to Dr. Seema Mital and Dr. Will Navarre as my committee members. Furthermore, during my experience in the STRIDE program at the Hospital for Sick Children, I had the wonderful opportunity to learn and be mentored by Dr. Mital on clinical aspects of cardiomyopathy. As a part of this program, I was able to learn and contrast my results in mice with data on human cardiomyopathy, with special guidance from Dr. Mark Friedberg in interpreting echocardiogram. Last but not least, I would like to thank all of our collaborators in this project: Dr. Benoit Bruneau for providing the *Irx4*KO mutants and his lab's preliminary work in the phenotypic assessment of the *Irx3;Irx4*DKO mutants, as well as Dr. Mark Henkelman's laboratory, especially Dr. Yu-qing Zhou, for performing Optical Projection Tomography.

Table of Contents

Acknowledgments.....	iii
Table of Contents.....	iv
List of Figures.....	vi
Chapter 1 Introduction.....	1
1 Introduction.....	1
1.1 Heart development and the compaction process.....	1
1.2 Left Ventricular Noncompaction.....	4
1.3 The heterogeneous genetic basis of LVNC.....	6
1.3.1 The Bmp10 pathway and its role in LVNC.....	7
1.3.2 Regulation of trabeculation and compaction involves various levels of cross-talk between different layers and regions of cardiac tissue.....	8
1.4 Iroquois family of homeodomain transcription factors in heart development.....	9
1.5 Rationale and hypothesis.....	11
Chapter 2 Materials and Methods.....	13
2 Materials and Methods.....	13
2.1 Mouse Lines and Genotyping.....	13
2.2 Histology.....	13
2.3 Echocardiogram Measurements and Analysis.....	14
2.4 Immunofluorescence staining and imaging.....	14
2.5 <i>In situ</i> Hybridization.....	15
2.6 Optical Projection Tomography and noncompact to compact myocardium ratio.....	16
2.7 Gene Expression Analysis.....	16
2.8 Immunoblotting.....	17
2.9 Statistical Analysis.....	17
Chapter 3 Results.....	18

3	Analysis of <i>Irx3;Irx4</i> mutants show a noncompaction phenotype.....	18
3.1	<i>Irx4</i> KO mutants display a subtle noncompaction phenotype	18
3.2	<i>Irx3^{+/-};Irx4^{-/-}</i> and <i>Irx3;Irx4</i> DKO mutants exhibit ventricular noncompaction	21
3.2.1	Mutant hearts with a functional copy of <i>Irx4</i> are phenotypically normal.....	21
3.2.2	<i>Irx3;Irx4</i> DKO mutants exhibit a partial postnatal lethality	22
3.2.3	Additional loss of <i>Irx3</i> exacerbates the noncompaction phenotype of <i>Irx4</i> KO mice in a dose-dependent manner.....	24
3.3	<i>Irx3;Irx4</i> DKO mice show systolic dysfunction and mitral regurgitation	27
3.4	<i>Irx3;Irx4</i> DKO mice show elevated expression of heart failure markers	31
3.5	Mutant mice exhibit myocardial and patterning changes at E14.5	32
3.5.1	<i>Irx3;Irx4</i> DKO mutants show thinner ventricular wall by E14.5	32
3.6	<i>Irx3;Irx4</i> DKO hearts have increased PECAM-positive endocardial cells, higher expression of trabecular markers, and a thinner layer of compact marker	32
3.7	Changes in molecular pathway are found in <i>Irx3;Irx4</i> mutants at E14.5 when compaction begins	34
3.7.1	<i>Irx5</i> is upregulated in the LVNC mutants.....	34
3.7.2	<i>Irx3;Irx4</i> mutants have altered <i>Bmp10</i> expression.....	35
Chapter 4	. Discussion	41
4	Discussion	41
4.1	Loss of <i>Irx3</i> exacerbates the noncompaction phenotype of <i>Irx4</i> KO mice.....	41
4.2	<i>Irx3;Irx4</i> mutant mice as a mouse model of LVNC	43
4.3	<i>Irx3;Irx4</i> mutants have altered <i>Bmp10</i> pathway expression which may contribute to noncompaction through continuous myocardial proliferation	46
4.4	Future Directions	48
References	50

List of Figures

Figure 1. General compaction process of the mammalian heart and the corresponding cellular layers	1
Figure 2. Common types of cardiomyopathy and their structural abnormalities	4
Figure 3. Embryonic and postnatal expression pattern of the <i>Irx</i> family of transcription factors	9
Figure 4. <i>Irx4</i> KO mice have a mild noncompaction phenotype	20
Figure 5. <i>Irx3</i> ^{+/-} ; <i>Irx4</i> ^{+/-} mutants have a normal phenotype comparable to the wildtype	21
Figure 6. All mutants with a functional copy of <i>Irx4</i> have normal morphology	22
Figure 7. <i>Irx3</i> ; <i>Irx4</i> DKO mutants show a partial postnatal lethality	23
Figure 8. <i>Irx3</i> ; <i>Irx4</i> DKO mice show a cardiac wasting phenotype	23
Figure 9. Dose-dependent loss of <i>Irx3</i> in an <i>Irx4</i> KO background increase noncompaction severity	25
Figure 10. Abnormal trabeculation and muscle structure are present in the <i>Irx3</i> ; <i>Irx4</i> DKO mice	26
Figure 11. Double mutants have collagenous deposits between muscle structures and abnormally long mitral valves	27
Figure 12. Echocardiography at P14 did not show significant differences in systolic function and wall thickness	28
Figure 13. Echocardiography at 5 weeks of age show significant changes in heart function	30
Figure 14. Heart failure markers are increased at 5 weeks in the <i>Irx3</i> ^{-/-} ; <i>Irx4</i> ^{-/-} heart	31
Figure 15. Ventricular wall is significantly thinner at E14.5 in <i>Irx3</i> ; <i>Irx4</i> DKO samples	32
Figure 16. <i>Irx3</i> ; <i>Irx4</i> DKO mice have expanded trabecular marker expression domain and a thickened endocardial layer	33
Figure 17. There is maintained upregulation of <i>Irx5</i> in <i>Irx3</i> ; <i>Irx4</i> DKO mutants	34
Figure 18. There is upregulation of <i>Bmp10</i> pathway genes at E14.5	35
Figure 19. Immunofluorescence analysis of mitotic marker phospho-histone H3 show increased cell proliferation in the left ventricular free wall of the <i>Irx3</i> ; <i>Irx4</i> DKO mice	37
Figure 20. <i>Bmp10</i> expression is upregulated at P21 but pathway activation only occurs in the absence of <i>IRX4</i>	39

Figure 21. IRX3 and IRX4 remain in the nucleus together prior to P5, but do not appear to bind each other 42

Chapter 1 Introduction

1 Introduction

1.1 Heart development and the compaction process

The heart is the first functional organ of the mammalian embryo and its proper formation is essential for growth and development¹. Heart development is a highly conserved process, and the sequence of heart formation is common to all vertebrate species², including the formation of the myocardial architecture in human and mice^{3,4}.

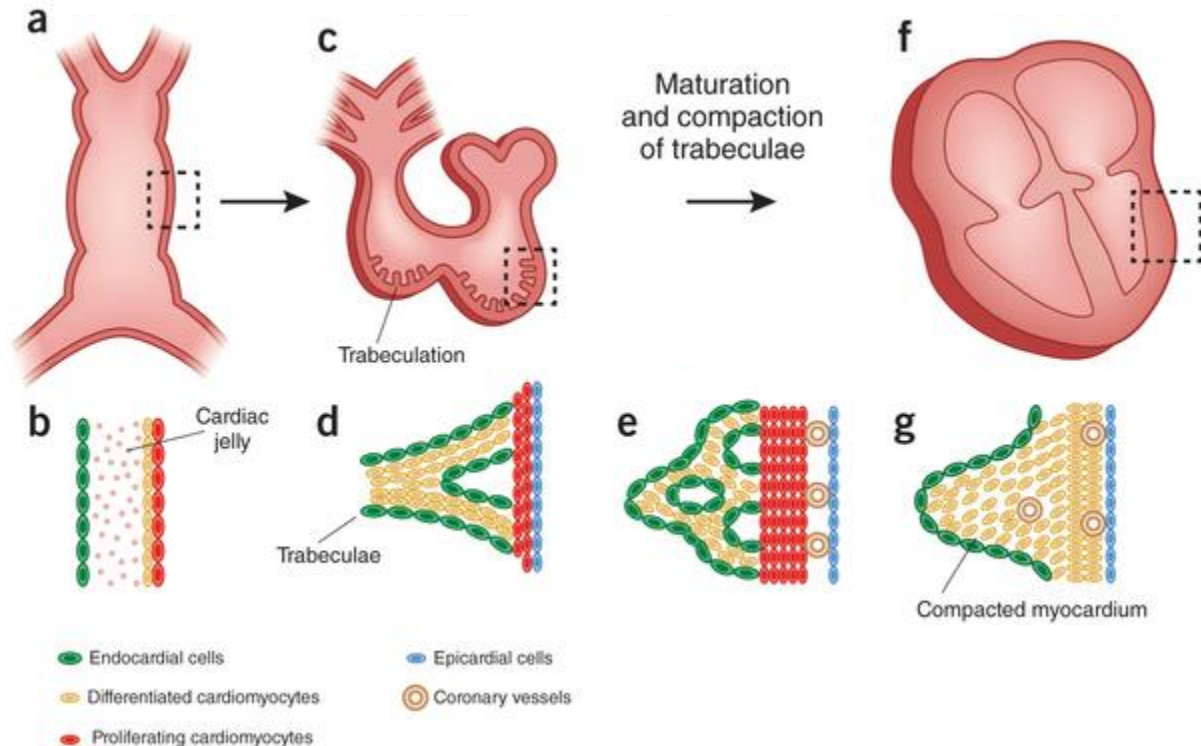


Figure 1. General compaction process of the mammalian heart and the corresponding cellular layers. The four stages comprising of linear heart tube (a, b), trabecular development (c, d), myocardial remodeling (e), and compact myocardium (f, g) are shown above. Adapted from Misra and Garg. Compacting the heart with Notch. *Nature Med.* 2013. 19:133-134.

First, the two cardiac mesoderm primordia fuse to form a linear heart tube by E8.5 in mice³. At this point, there is a single layer of myocardial cells and one cell layer of endocardium lining the

lumen of the tube, and between these two layers is the cardiac jelly rich with extracellular matrix⁵. Second, when the tube undergoes looping, the two ventricular chambers begin to form, generally around E9.5⁵. The outside layer of the myocardium is organized into compact myocardium. Trabeculae are the thin, sheet-like, myocardial projection into the chamber, and they form at E10.5 from trabecular ridges³. The current theory regarding this process involves the active invagination of the myocardium, driven by the delamination of the compact myocardium from the primary trabecular ridges⁶. This dramatically increases the surface area of the myocardial mass, helping to facilitate oxygen exchange in the absence of coronary circulation³. This meshwork of trabeculation is thought to derive from the underlying compact ventricular wall⁷, rather than through proliferation within the trabecular mesh itself, because proliferative activity has been consistently shown to be higher in compact myocardium and cardiomyocytes are more differentiated towards the trabecular side^{3,8}. P57^{kip2}, a cyclin-dependent kinase inhibitor, is specifically expressed in the trabeculae to inhibit cell cycle progression⁹. Therefore, it appears that a spatial balance of proliferation and differentiation is essential for myocardium development. Third, by E14.5, when the coronary circulation is established and septation is completed, remodeling in the form of compaction begins³. This process refers to the trabeculae compressing downwards to become a part of the ventricular wall, from about 2-4 cell layers thick into a denser, solid muscular structure suitable for pumping³. Whether this process is mediated by resorption or remodeling is still unclear¹⁰. One possibility is that trabeculae stop growing and instead thicken and collapse into the myocardial wall¹⁰. Compaction should be mostly finished by E16.5 and cardiomyocyte maturation and the muscular structure continue to be refined into the late fetal and neonatal stages of mouse development⁵.

Other notable muscular structures in the heart include the septum and papillary muscles. The interventricular septum is the muscle dividing the left and right ventricles, preventing mixing of oxygenated and de-oxygenated blood. While the septum is formed by fusion of trabecular sheets in avians¹¹, in mammals this structure arises in response to the upward force associated with apical growth¹². Papillary muscles are conical muscular structures that connect the ventricular wall to the inflow valves through connective tissues called chordae tendineae. The function of these muscles is to hold the valves closed during heart contraction in order to prevent the backflow of blood into the atria. The detailed developmental mechanism responsible for the formation of these muscles is largely unknown. Based on morphological observations, it is

speculated that these muscles develop through a combination of coalescence of trabeculation³ and delamination to form a segregated muscle structure only attached to the wall at its base¹³.

The properly formed muscular structure of the mammalian four-chambered heart is critical for pumping blood throughout the body. Blood from the systemic circulation arrives at the heart through the superior and inferior vena cava into the right atrium. It then travels into the right ventricle and is pushed into the pulmonary circulation for re-oxygenation. From the pulmonary artery, oxygenated blood moves back into the heart at the left atrium. During heart relaxation, or diastole, the blood is drawn into the left ventricle due to the low pressure there in comparison to the left atrium as the volume expands. This path is gated by the mitral valve, a bicuspid valve anchored by the two papillary muscles in the left ventricle to hold it closed during heart contraction. Systole, which refers to the contraction of the ventricles, pushes blood from the left ventricle into the systemic circulation through the aorta. At this time, due to the papillary muscles pulling tautly on the mitral valve, the high pressure blood flow is unable to enter the left atrium from the left ventricle. If backflow of blood into the left atrium occurs at this time, a process termed mitral regurgitation, then a higher volume of blood and pressure results in the left atrium¹⁴.

The laboratory mouse is a well-established model for studying cardiomyopathy. Qualitative categorizations such as Theiler stages, developmental process, heart morphology, and major mechanisms influencing heart development in mice are highly comparable to those of humans, with only subtle differences³. One difference worth noting is that some developmental processes, mainly the delamination and myocardial remodeling processes, are still being refined in the mouse hearts after birth¹⁵. In addition, small morphological differences are present in the venous pole. Otherwise, humans and mice are remarkably similar in terms of developmental events that guide heart formation¹⁵. They are also similar in their physiological responses to heart failure. In humans, heart failure is characterized by organ failure due to insufficient blood flow, with symptoms like exertional dyspnea, orthopnea, and lower extremity edema¹⁶. While not a part of the preliminary diagnosis, expression of diagnostic heart failure markers in the blood, alpha-actinin, atrial natriuretic protein (ANP), and brain natriuretic protein (BNP), are used regularly to monitor the progress of heart failure¹⁷. In mice, as it is difficult to monitor physical symptoms, the expression of heart failure markers in blood or heart tissue is often used as a diagnostic tool. Furthermore, many evaluative techniques used in humans can be applied to mice. Lastly, a

mammalian model is especially suitable for studying noncompaction because the persistence of spongy myocardium is often seen in the ventricular walls of fish and reptilian, consistent with normal circulatory function in these systems¹⁸.

1.2 Left Ventricular Noncompaction

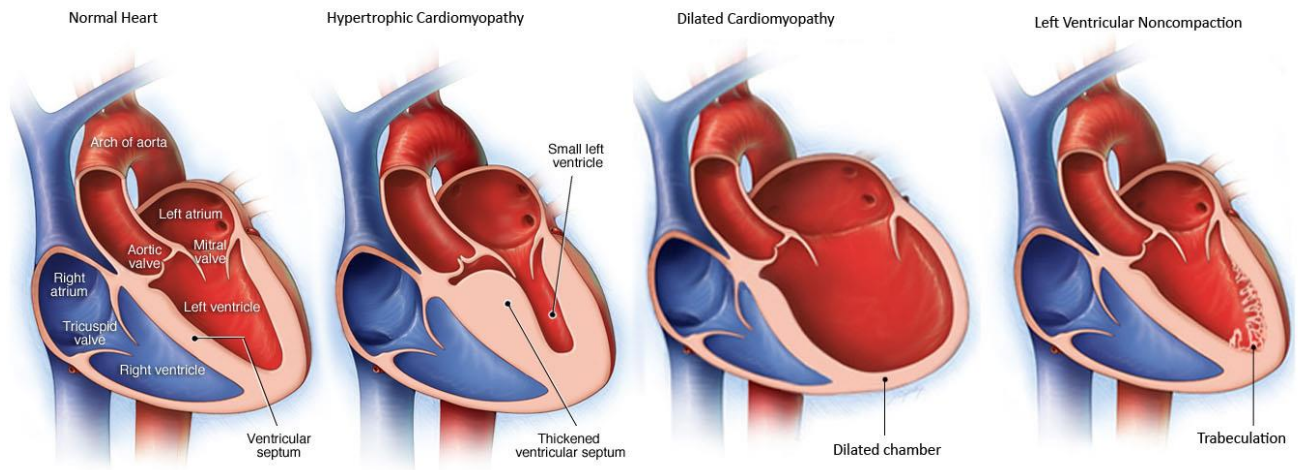


Figure 2. Common types of cardiomyopathies and their structural abnormalities. Compared to the normal heart, hypertrophic cardiomyopathy is characterized by a thickening of the ventricular wall and septum, dilated cardiomyopathy results in the ballooning of the ventricular chamber, and left ventricular noncompaction have distinct trabecular projections in the left ventricular chamber. Adapted from www.mayoclinic.org.

LVNC is characterized by excessive trabeculation of the luminal surface of the left ventricle, and sometimes the right ventricle as well¹⁸. It has been classified by the American Heart Association as a primary, genetic, congenital cardiomyopathy^{19,20}. Indeed, about 40%²¹-67%²² of the cases are familial. It is the third most common cardiomyopathy after dilated cardiomyopathy and hypertrophic cardiomyopathy²³. LVNC has been gaining attention in recent years, in part because its increased detection via sophisticated imaging techniques^{18,24}. First described in 1926²⁵, its prevalence has been estimated from anywhere between 1 to 26 in 10,000 individuals^{18,20,22,24}.

LVNC can be clinically noted at any point during a person's life, *in utero* as well as postnatally^{18,20,26}. The morphology of noncompaction is also variable, and LVNC often presents

with other diseases and cardiomyopathies, e.g. Barth syndromes and endocardial fibroelastosis^{18,20}. Currently, the term “isolated LVNC” specifies LVNC without distinct cardiac co-morbidities¹⁸. While patients can be asymptomatic, most often they develop heart failure (failure of the heart to efficiently pump blood throughout the body), thromboembolic events (due to blood clots forming between the trabecular gaps), or tachyarrhythmia (due to disruption of the conduction network in the myocardium)¹⁸. The gold standard for diagnosis of LVNC is through measurement of the noncompact to compact myocardium thickness in echocardiography. While the specific criteria varies across hospitals and cardiologists¹⁰, including the number of measurements and the area of measurement, diagnosis of noncompaction in humans typically requires a noncompact to compact ratio (NC:C) of more than 2 through echocardiography or 2.3 through cardiac MRI²⁷. What this means is the distance from epicardial surface to peak of the trabeculation is more than double the distance between base of the trabeculae and epicardial layer²⁰. Other criteria such as more than 3 noncompact regions and presence of blood flow between the intertrabecular recesses through Doppler Echocardiography have also been suggested^{26,27}. It should be noted that the amount of trabeculation also varies in normal ventricles, with a diverse range of ratios found in different regions of the ventricle¹⁸. In fact, there is usually a greater proportion of trabecular myocardium at the base of papillary muscles and in the apex. The specific pattern of trabeculation is also unique to each individual³, and a range of NC:C ratio of health myocardium is expected. However, the NC:C ratio does not normally exceed 1, even in these regions and cases¹⁸.

It has been suggested that there are distinct phenotypes within LVNC and it should be further classified²⁴. While thick and prominent coarse trabeculation is frequently present in all LVNC cases²⁸ and the underlying microscopic features are similar²⁹, the specific pattern and thickness of the diseased myocardium vary in the literature. By gross patterning of the myocardial structure in the noncompact layer, Burke *et al.* has recommended three main subclasses²⁹: anastomosing trabeculae that resemble irregularly branching muscle bundles; spongy trabeculae that contain a dense meshwork of interlacing smaller muscle bundles; and polypoid trabeculae that resemble multiple papillary muscles within the left ventricle. Out of the 14 cases studied by Burke *et al.* representing sudden death of infants, six were labeled as the polypoid pattern of noncompaction, suggesting that either this pattern is more common or it may have a higher correlation with sudden pediatric cardiac death. While this classification is only starting to take

root in the literature and is not yet widely accepted, it's supported by genetically modified mouse models. Specifically, there appears to be a range of disease morphology as well as differences in molecular basis. For example, 'hypertrabeculation' is characterized by increased trabeculation from an early embryonic time point, and this is likely associated with normal ventricular wall thickness. The phenotype of these models, such as Notch2-overexpression mice³⁰ and *Nkx2.5*-deficient hearts³¹, often appear more closely related to the spongy trabeculae pattern. Second, 'noncompaction' occurs when trabecular growth proceeds as normal but trabecular remodeling to a compact structure is hindered after trabecular growth. Other models, such as the *tafazzin*-knockdown mice, *SRC-1*;*SRC-3*DKO mice and *Mib1*^{fllox};*cTnT-cre* mice, show normal amounts of trabeculae during early embryonic development, yet a thinner ventricular wall with residual trabeculation by later stages. The phenotype for these models are more similar to the anastomosing and polypoid patterns of noncompaction. However, classification is difficult as it is a subjective process and current models, such as the FKBP12 KO mice³², can also exhibit both phenotypes. In humans, most evidence supports the cause of LVNC to be a failure to remodel the trabecular network¹⁸, while in mice, as described in more detail below, LVNC phenotype appears to arise from altered proliferation patterns of cardiomyocytes. Whether these two deficiencies are related or reflect a difference between species is still a large unknown in the field.

1.3 The heterogeneous genetic basis of LVNC

LVNC is a genetically heterogeneous disease²⁴. Genetic screening in humans has identified mutations in genes mostly involved in contractile function and sarcomeric proteins such as beta-myosin heavy chain as well as alpha-cardiac actin²⁴. However, exactly how these mutations contribute to ventricular noncompaction during embryonic development is not known, nor do they predict clinical phenotypes³³. About a dozen published mutant mouse models are known to exhibit a noncompaction heart phenotype^{6,22,30,32,34-39}. The vast majority of these mutants display other heart anomalies such as atrial septation defect³¹. While they reflect the human disease spectrum, how these genes and their associated signaling pathways control the basic compaction process, and contribute to disease conditions remains to be deciphered. Nevertheless, these studies suggest that ventricular compaction is controlled by many signaling pathways and likely involves cross talk between distinct pathways⁵.

1.3.1 The Bmp10 pathway and its role in LVNC

Bone morphogenetic protein 10 (Bmp10) is a member of the TGF-beta superfamily⁷. It is a positive regulator of cardiomyocyte proliferation, likely through its negative regulation of *Cdkn1c*⁷, which codes for the cell cycle inhibitor p57^{kip2}. Bmp10 acts on the ALK1 receptor, which in turn phosphorylates SMAD1/5/8, leading to nuclear translocation and activation of target gene expression. *Bmp10* is highly expressed in the trabecular myocardium transiently between E9.0 and E13.5, but is restricted to the right atrium postnatally⁷. As it signals to the trabecular base, it has to be turned off in the trabecular regions to restrict cellular proliferation, right before compaction begins to take place⁵. By acting on the basal layer, Bmp10 restricts p57^{kip2} to the trabecular region, directly inhibiting its expression through a SMAD binding site. This results in myocardial proliferation at the trabecular base and timely cell cycle exit of trabecular cardiomyocytes³⁴.

Bmp10 KO mice die around E10.5 due to poorly developed hearts. Mutant hearts show profoundly reduced proliferation resulting in hypoplastic ventricular walls without trabeculae despite the formation of primitive trabecular ridges. P57^{kip2} is upregulated and ectopically expressed in mutants, leading to reduced cell proliferation⁷. Overall, these results indicate that Bmp10 is not needed for initiation of cardiac trabeculation, but is essential for its subsequent growth³⁵. As trabeculation is likely derived from the proliferative cardiomyocytes at the trabecular base, these observations also provide evidence that Bmp10 signals to the cardiomyocytes at the trabecular base.

Perturbations to the Bmp10 pathway have been implicated in several mouse models of LVNC. FKBP12 KO mice represent the first model for isolated LVNC⁴⁰ and exhibit heart phenotypes characteristics of both hypertrabeculation and noncompaction⁵. FKBP12, a member of the immunophilin family, forms complexes with many proteins including BMP/activin/TGF-beta type-I receptors^{40,41}. FKBP12 KO mice show trabeculation and compaction phenotypes as early as E11.5. They die between E14.5 and birth, displaying a wide range of morphological defects including increased number and thickness of trabeculation, intertrabecular recesses, lack of compaction, as well as ventricular septal defect³⁵. A closer look at E18.5 mutant hearts revealed thickened trabecular structures that resemble muscle bundles. In these mutants, *Bmp10* is highly up-regulated, expressing in both trabecular and compact wall regions. The up-regulation of

Bmp10 is also associated with reduced *Cdkn1c* expression and increased proliferation of trabecular myocardium⁷. Consistent with this, mice with *Bmp10* overexpression also develop cardiac hypertrabeculation and noncompaction similar to FKBP12-deficient hearts^{5,35}.

FKBP12 has been recently found to regulate Notch signaling, whereby Notch 1 activity is enhanced in FKBP12 KO mice and inhibition of Notch partially rescues the hypertrabeculation phenotype³². Similarly, overexpression of activated Notch1 resulted in ventricular noncompaction, among other congenital heart defects⁴². Notch1 itself and other Notch ligands are expressed in the endocardium near the base of the developing trabeculae⁴³. It has been shown that Notch regulates trabeculation via *Bmp10* in cardiomyocyte proliferation, and neuregulin 1 (*Nrg1*) in cardiomyocyte differentiation³⁶. Correspondingly, mouse mutants with elevated Notch activity are associated with hypertrabeculation and noncompaction⁵. Indeed, *Bmp10* is upregulated in mice deficient for *Numb/Numb-like*, which regulate endocytosis of Notch³⁰. In addition, myocardial-specific *Nkx2.5* KO mice also showed upregulation of *Bmp10* and cardiomyocyte proliferation, where *Bmp10* was found to be necessary and sufficient for the hypertrabeculation phenotype³¹. Collectively, these studies demonstrate that trabecular proliferation is associated with ventricular compaction.

1.3.2 Regulation of trabeculation and compaction involves various levels of cross-talk between different layers and regions of cardiac tissue

Signaling between endocardium, epicardium, and myocardium is critical for ventricular wall development and trabecular growth. For example, *Nrg1* is produced in endocardial cells and triggers a signaling cascade in myocardial cells through the receptors ErbB2/ErbB4 to promote cell proliferation³⁷ and control delamination to initiate trabecular development⁶. Some growth factors involved in epicardial and coronary vasculature development are also involved in trabeculation. For example, vascular endothelial growth factor (VEGF) and angiopoietin signal from myocardium to endocardium to regulate trabeculation⁴⁴. Epicardial FGF/myocardial FGF receptor signaling is involved in ventricular wall development⁴⁵. Interestingly, while epicardial-derived growth signals affect compact myocardium markers, endocardial-derived growth signals play a more important role in the expression of trabecular myocardium markers⁴⁶. The cardiac jelly also plays a role in trabecular development. For example, deregulation of ADAMTS1 in the endocardium causes premature breakdown of this matrix, resulting in early termination of

trabeculation³⁸. These observations suggest that multiple secreted factors and their signaling pathways play intricate roles in the intercellular regulation of trabeculation and compaction.

1.4 Iroquois family of homeodomain transcription factors in heart development

For the proper formation of the heart, a complex network of transcription factors act at specific times and locations. The Iroquois (Irx) family of TALE homeobox transcription factors are key regulators in many developmental processes, including heart development¹. Originally described in *Drosophila*, this family is highly conserved between organisms⁴⁷. In mammals, there are six members, named *Irx1-6*, and they are located in two genomic clusters. *Irx1*, *Irx2*, and *Irx4* are in cluster A and *Irx3*, *Irx5*, and *Irx6* are in B^{1,47}. The six family members are all expressed throughout the heart during development⁴⁷, and some are implicated in functions such as establishment of chambers and ventricular repolarization¹.

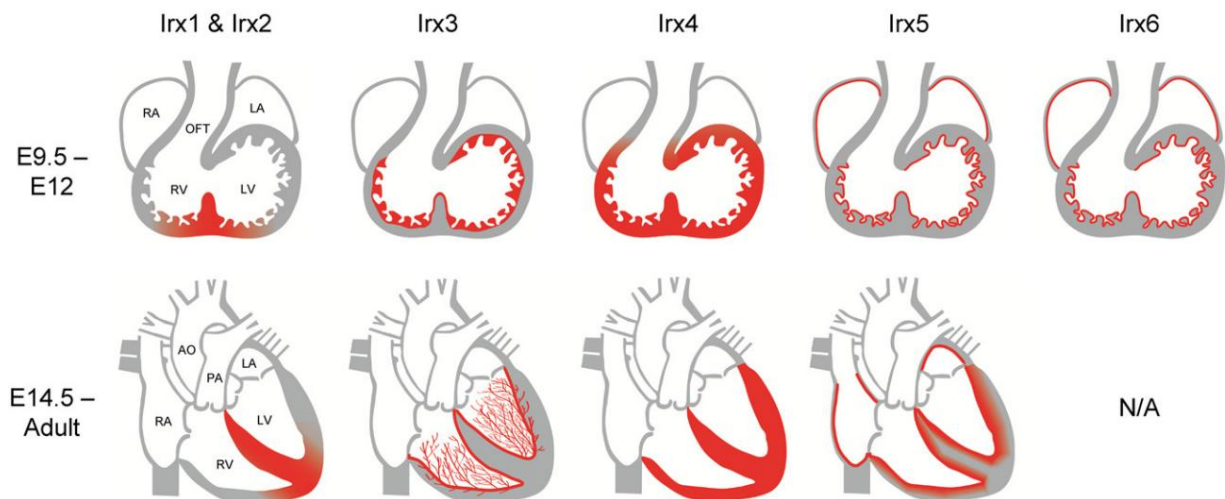


Figure 3. Embryonic and postnatal expression pattern of the Irx family of transcription factors. The six family members are expressed during heart development in both overlapping and unique patterns with other family members. RA and LA refer to right and left atrium, AO for aorta, PA for pulmonary artery, and RV and LV for right and left ventricle. Adapted from Kim *et al.* (2012). Iroquois homeodomain transcription factors in heart development and function. *Circ Res.* 110:1513-1524

The *Irx* family of transcription factors exhibit distinct, as well as overlapping functions¹. *Irx3*, *Irx4*, and *Irx5* have been characterized in more detail while the functions of the other members, *Irx1*, *Irx2*, and *Irx6* are still unknown. Of the latter three, *Irx1* and *Irx2* have identical patterns of expression in the trabeculated myocardium that coincides with regions where atrioventricular (AV) bundle and bundle branches are formed⁴⁷. As such, while the *Irx1*KO phenotype is unknown, *Irx2*KO mice do not display a heart phenotype. The lack of a heart phenotype in *Irx2*KO mice may be due to the functional redundancy of *Irx1* and *Irx2*⁴⁷. In comparison to the rest of the family, *Irx6* is expressed relatively at a lower level, but follows the *Irx5* expression pattern. The function of *Irx6* in cardiac development, if any, is currently unknown. *Irx6*KO mice do not display any cardiac phenotypes (unpublished).

In the better studied half of the family, *Irx3* is only expressed in the trabecular regions of the heart and is often used as a marker for trabecular identity⁴⁸. *Irx3* is essential for Purkinje cell development and postnatal maturation. *Irx3* is also expressed in a subset of developing trabeculae and cells surrounding the emerging interventricular septum by E11. After E14, *Irx3* is expressed in the His bundle primordium, bundle branches in the septum, and trabeculae. In the adult heart, *Irx3* marks the His bundle and its branches. Specifically, *Irx3* is highly expressed in the specialized His-Purkinje system cells and regulates the expression of gap junction genes *Gja1* and *Gja5*, through direct repression and indirect activation, respectively. Through this, *Irx3* is able to control electrical maturation and synchronicity of ventricular depolarization. In the *Irx3*KO heart, there is a blockage of the right bundle branch due to conduction slowing in the cells lacking *Irx3*. These mice show a cardiac conduction defect by 2 weeks of age when they display prolonged ventricular activation⁴⁹. Independent of gap junction gene regulation, *Irx3* also controls the maturation of the ventricular conduction system: conduction fiber densities were severely reduced in *Irx3*KO hearts. By regulating cell cycle exit required for recruitment and differentiation of mature ventricular conduction cells, *Irx3* is essential for the proper formation of the ventricular conduction system⁵⁰. Consistent with these mouse studies, *IRX3* mutations have also been identified in humans with idiopathic ventricular fibrillation with impaired *Gja5* expression⁵¹.

Irx4 is a marker for ventricles across species, including chicken, mice, and humans. Indeed, it is one of the earliest markers of ventricular precursors and expressed in the ventricular myocardium throughout development⁵². This gene is important for establishing ventricular identity at least

partially, by regulating expression of ventricular specific genes including *eHand*, and down-regulating atrial-specific genes like *ANF*. The heart morphology of *Irx4*KO mice (at birth and early postnatal period, including those at P10) was reported to be normal⁵³. However, these mutants develop atrial enlargement by 6 weeks of age, suggesting right ventricular dysfunction⁵³. By echocardiography, they exhibited increased end-systolic volumes and a decreased ejection fraction. Therefore, *Irx4*KO hearts show adult-onset myocardial hypertrophy, chamber dilation, and systolic dysfunction. In humans, *IRX4* mutations have been associated with two familial cases of ventricular septation defect⁵⁴.

Irx5, expressed in the endocardium lining trabeculae¹ and septum⁵⁵, contributes to endocardial cushion formation⁴⁷. The gradient of *Irx5* negatively regulates potassium channel Kv4.2 expression in the heart to establish the gradient facilitating the orderly sequence of repolarization⁵⁶. *Irx5*KO mice are viable, fertile, and their hearts are morphologically normal⁵⁶, but they are highly susceptible to induced ventricular tachyarrhythmia⁵⁶.

Irx family members' overlapping expression often translates into functional redundancy. For example, both *IRX3* and *IRX5* have been shown to repress *Bmp10* expression in the endocardium as well as control AV conduction postnatally⁵⁵. *IRX3* and *IRX5* have redundant functions as *Irx3/5*DKO mice die *in utero* around E14.5 from malformations including improper outflow tract orientation, absence of dorsal mesenchymal protrusion, double outlet right ventricle, and ventricular septum defects at the AV canal⁵⁵. Some lines of evidence also suggest possible overlapping functions between *IRX3* and *IRX5* with *IRX4*. For example, *IRX4* can also interact with mBop, the corepressor known to bind to *IRX5*⁵⁶. Additionally, *in vitro* studies showed that *IRX4* can physically interact with *IRX3* and *IRX5*⁵⁵.

1.5 Rationale and hypothesis

This precedent in cooperative function of *Irx* family members presents the possibility of other such interactions. *Irx3* and *Irx4* emerge as possible candidates because they also share expression domains in the trabecular region⁴⁷, and both have been associated with LVNC. *Irx3* did not show any morphological defects but is known to regulate *Bmp10* expression directly, as revealed by ChIP and luciferase assays⁵⁵. *IRX3* inhibits *Bmp10* expression and *Bmp10* expression is correspondingly upregulated within the trabecular regions of the *Irx3*KO mutants. However, while *Bmp10* expression was upregulated in *Irx3*KO hearts by more than 40-fold, which should

be enough to induce noncompaction as suggested by other published studies, LVNC was not observed in *Irx3*KO mice⁵⁵. This suggests that *Bmp10* upregulation is not sufficient for inducing noncompaction, and additional factors or pathways regulating cardiac compaction are involved. Our preliminary studies on *Irx4*KO mice (explained in further detail in the Results section) unveiled a slight noncompaction phenotype that was not described in previous studies. Thus, we hypothesized that *Irx3* and *Irx4* may possess overlapping functions critical for trabecular compaction, and ablation of both *Irx3* and *Irx4* in the developing mouse heart may result in an exacerbated LVNC phenotype.

Chapter 2 Materials and Methods

2 Materials and Methods

2.1 Mouse Lines and Genotyping

Irx3^{taulacZ} mutant mice as described in Zhang *et al.*^{48,55} were crossed with the *Irx4*KO mutant mice as described in Bruneau *et al.*⁵³. Mutants were maintained in a mixed CD1 background. Genotyping was performed by PCR using *Irx3* primers (Wildtype forward: 5' GAGTTGGCCGCCTCTGGGTCCCTATCCAAT 3', Wildtype reverse: 5' CCCTCTCTCCCGGGTTTCTCTGGCTCTTAC 3' and mutant reverse: 5' ACCTCCCACACCTCCCCCTGAACCTGAAAC 3') and *Irx4* primers (Wildtype forward: 5'GCGGGTGCGGCCTAAGAAG 3', wildtype reverse: 5' TTGAGCAGCATATGGGTGAACTAA 3' and mutant reverse: 5'GCGCTACCGGTGGATGTGGAATGT 3'). Animals were cared for in accordance with national requirements with the approval of The Hospital for Sick Children Animal Care Committee.

Only male mice were studied in detail and quantified for the data presented in the thesis, as female mice showed variable measurements in heart function due to body and hormone difference. It is important to note that mice of both genders showed the same noncompact heart structures.

2.2 Histology

Embryos were harvested from timed mating, where the midday following the presence of a vaginal plug was considered embryonic day 0.5 (E0.5). Pregnant females were sacrificed by cervical dislocation and embryos were dissected in cold phosphate buffered saline (PBS). Whole embryos were fixed in 4% paraformaldehyde (PFA) overnight, followed by dehydration using ethanol series and embedding in paraffin at 65 °C. Four chamber and two chambered view microtome sections (6-7 µm) were stained with Hematoxylin and Eosin (H&E), Masson's Trichrome Stain, and X-gal using standard methods.

The NC:C ratio was calculated by using three measurements of the histological sections from three samples per genotype.

2.3 Echocardiogram Measurements and Analysis

Echocardiography of mice at postnatal day 14 and 5 weeks was performed using a Vevo 2100 System (Visual Sonics). Mice were anesthetized using 2% isoflurane and placed in a supine position. Temperature was monitored using a rectal temperature probe and kept between 37 °C to 38 °C. Fur was removed from the chest using an electric clipper followed by a depilatory agent (Nair). Long-axis M-mode 2-dimensional echocardiography was obtained perpendicular to the midventricular level. It was used to visualize the systolic function and wall function²⁶. Colour Doppler Mode detected blood flow directionality and velocities of the mitral flow⁵⁷. As timing of the events was more important, a window closer to the parasternal short axis was used to achieve the best mitral valve flow. The scale, baseline, and filter were not changed between animals. VevoStrain Analysis software was used to measure and quantify the data.

To analyze left ventricular dimensions and systolic performance from M-mode echocardiography, wall trace was performed in two recordings per heart sample, where three traces were done for a duration of four heartbeats. Thus the calculations are an average of 24 contractile motions for each sample. Due to the noncompact nature of the heart wall for select genotypes, determination of the wall boundaries was subjective. To be consistent between samples, the analysis was performed by one individual with the first discrete and continuous line always used as the wall edge. Comparisons of the calculated values were also made against values calculated from additional separate measurements of the septal thickness, left ventricular chamber length, and posterior wall thickness to ensure similar and consistent findings.

Mitral valve function were quantified by tracing the blood flow pattern in the velocity-time graph to generate the E and A wave values, valve deceleration speed was determined as the initial velocity of closure immediately after the E wave, and valve deceleration time was measured as the peak of the E wave to the initiation of the A wave⁵⁷.

2.4 Immunofluorescence staining and imaging

For immunofluorescence staining, OCT frozen samples were cryoprotected using 30% sucrose before OCT embedding. Serial 4 chambered view cryosections (7 µm) were blocked with

blocking solution (10% serum, 0.3 M glycine in TBST) for 1 h. Slides were stained with primary antibodies against *Irx3* (1:100, Novus Biologicals), phospho-histone H3 (1:100, Cell Signalling), and phospho-SMAD1/5/8 (1:100, Cell Signalling Technology) diluted in blocking solution overnight at 4 °C in a humidified chamber. Secondary staining was achieved using appropriate Alexa-conjugated antibodies (Invitrogen) for 1 h at room temperature. DNA counterstaining and mounting were done using Vectashield Hardset Mounting Media (Vector Laboratories). Images were taken using Nikon Eclipse Ti scanning confocal microscope and subjected to quantification and statistical analysis.

To visualize the proliferation pattern, the left ventricle at E13.5 was divided into five arbitrary segments labeled as the septal, basal, mid-basal, mid, and apical regions, as described further in the Results section. Total number of cells and pH3 positive cells in each region were counted at a 60x magnification to generate the percentage of pH3 positive cells (three samples per genotype). In our studies, the rate of pH3 positive cells appeared lower than those in the literature (around 8-10% at E14.5^{36,58}). However, it should be noted that depending on the experiments and methods, a wide range of mitotic rates have been reported using pH3 staining, from 2%⁵⁹ to 20%⁶⁰ at E14.5. As well, preliminary data using wildtype samples show that while paraffin embedded sections have a pH3-positive rate of about 2%, OCT-embedded sections have a rate of about 6% in the same distribution, signifying that while the rate of proliferation differs between the conditions, the pattern of proliferation remains stable.

2.5 *In situ* Hybridization

In situ hybridization was carried out as described by Mo *et al.*⁶¹ on paraffin-embedded sections (7 µm). Digoxigenin-dUTP (DIG)-labelled RNA probes for *Irx3*, *Nppa*⁴⁷, *Bmp10*, *Tbx20*⁵⁵, *cTnI* (sense: 5' CGATGCGGCTGGGGAAC3', antisense: 5' TTCAGAGCACAGTGTGGGAG 3'), and *Pecam* (sense: 5' CGACCCTAAGAACGGAAGGC 3', antisense: 5' GCTGGCTTGAGGTCTGTCTT 3') were synthesized as previously described⁶².

2.6 Optical Projection Tomography and noncompact to compact myocardium ratio

Postnatal day 14 mice were placed under anesthesia (4% isoflurane, PPC) and their hearts were perfused with 4% PFA to clear the blood. Optical Projection Tomography (OPT) was performed as described^{63,64}.

Quantifying the NC:C ratio using 2D short-axis slices from the generation of the OPT model was done by taking a slice from each of the three (Basal, Mid, and Apical) regions of the heart (three samples per genotype). In total, this resulted in 9 slices per genotype. For each slice, three measurements were made of the noncompact and compact distance; one from the least compact region, most compact region, and an average compact region determined by eye. In total, the average of 27 measurements of NC:C ratio encompassing different levels and compaction regions of the heart were made. While this method would get a lower value than conventional measurements using only noncompacted areas²⁸, it provided a more holistic assessment.

2.7 Gene Expression Analysis

Total RNA was isolated using TRIzol reagent (Invitrogen) according to manufacturer's instructions. RNA was reverse transcribed into cDNA using the MMLV system (Thermo Fisher Scientific). Primers for mouse *Irx3* (forward: 5' CGGAGAGTGGAACAGATCGC 3', reverse: 5' CTGATAAGACCAGAGCAGCGT 3'), *Irx4* (forward: 5' CCCGCCATGTCCTACCCGCAGTT 3', reverse: 5' GCAGGCCCGGAATCAGCCAGTGTG 3'), *Irx5* (forward: 5' GGCTACAACCTCGCACCTCCA 3', reverse: 5' CCAGGAACCTGCCATACCG 3'), *Gapdh* (forward: 5' TCGTCCCGTAGACAAAATGG 3', reverse: 5' GAGGTCAATGAAGGGGTCGT 3'), *Nppa* (forward: 5' CGTCTTGGCCTTTTGGCTTC 3', reverse: 5' GGTGGTCTAGCAGGTTCTTGAAA 3'), *Act1* (forward: 5' CTCTCTCTCCTCAGGACGACAATC 3', reverse: 5' CAGAATGGCTGGCTTTAATGCTTC 3'), *Myh7* (forward: 5' ATGTGCCGGACCTTGGA 3', reverse: 5' CCTCGGGTTAGCTGAGAGATCA 3'), *Bmp10* (forward: 5' GAACGAAGATCTGTTTTCTCAACCA 3', reverse: 5' TTTACGGTCCACGCCATCA 3'), *Notch1* (forward: 5' GATGGCCTCAATGGGTACAAG 3', reverse: 5' TCGTTGTTGTTGATGTCACAGT 3'), and *Tbx20* (forward: 5' GTGCACATCATAAAGAAGAAAGACC 3', reverse: 5'

AAACGGATTGCTGTCTATTTTCAGC 3') were used with Power SYBR Green Master Mix (Applied Biosystems). Three independent RNA samples were isolated for each genotype and each reaction was repeated in triplicates for technical control. Results were normalized to *Gapdh* (endogenous control) and analyzed using the $2^{-\Delta\Delta CT}$ method. Reported values (fold increase) are means of three individual samples at postnatal stages and six samples at E14.5.

2.8 Immunoblotting

Heart tissue was dissected on ice and lysed using Hepes Lysis Buffer (20 mM Hepes pH7.5, 150 mM NaCl, 1 mM EGTA, 1% Triton X-100) supplemented with protease inhibitor cocktail tablet (cOmplete Mini, EDTA-free, Sigma Aldrich) in the Mini-beadbeater (Sigma Aldrich) for 30 seconds on, 2 minutes off, until all tissues were homogenized. For immunoblotting, tissue lysate concentrations were measured using the Bradford Assay (BioRad) and 50 μ g were loaded per lane) in a 10% SDS-PAGE gel. Gels were run for 0.5 h at 70V and 1.5 h at 120V. They were transferred at 4 °C at 100V for 1.5 h and blocked with 5% milk in TBST. Overnight incubation in primary antibodies *Irx3* (1:1000 Santa Cruz) and *Irx4* (1:1000 Abcam) was followed by detection using SuperSignal West Femto Chemiluminescent Substrate (Thermo Fisher Scientific).

2.9 Statistical Analysis

Differences between groups were examined for statistical significance by ANOVA followed by Tukey's post hoc test. *P* values of <0.05 were regarded as significant.

Chapter 3 Results

3 Analysis of *Irx3;Irx4* mutants show a noncompaction phenotype

Preliminary studies from Dr. Bruneau's lab suggested *Irx3;Irx4*DKO mutants have an embryonic lethal phenotype, perishing between E12.5-E14.5. One sample displayed a ventricular septation defect and they saw an expansion of the *Irx3* expression domain into the muscular septum in the double-knockouts. Upon undertaking further studies on these double mutants, we were surprised to see that double knockouts can survive postnatally and the scope of their heart defect goes beyond the septation process, as described in this chapter in further detail.

The morphological phenotyping of all the mutant hearts proceeded through the same pipeline. First, histological analyses were used to initially determine the 2-dimensional gross morphology of each of the mutants. Echocardiography was then used to confirm the morphology, quantify the cardiac function, and image the blood flow. Lastly, Optical Projection Tomography was performed to make a high-resolution 3D model of the heart, allowing for deeper understanding of the structures and more accurate measurements.

3.1 *Irx4*KO mutants display a subtle noncompaction phenotype

In the process of phenotyping *Irx3;Irx4*DKO mice, we first examined the single KO mice using the same protocol in order to make fair comparisons. As previously mentioned, neither *Irx3*KO nor *Irx4*KO mice were expected to have any congenital malformations. While this was true for *Irx3*KO mice, which did not exhibit any apparent morphological differences compared to wildtype, we identified a subtle noncompaction phenotype in *Irx4*KO mice. Noticeably, *M*-mode echocardiography of *Irx4*KO hearts at P14 and 5 weeks showed some extraneous muscle projections into the ventricular chamber. The posterior wall, instead of a clear discrete white line, showed multiple faint lines indicative of extra projections into the chamber and an overall less compacted structure (Figure 4a). This was confirmed by OPT showing the presence of trabeculation, muscle branches at the base of the papillary muscle, and increased distance between the papillary muscles to the ventricular free wall. Quantification of the noncompact to compact ratio (NC:C) in the mutants using raw OPT data unveiled an increased ratio of 0.77

compared to that found in wild-type (0.55) and double heterozygous mutant mice (0.56) (Figure 4b). By histological sectioning and H&E staining at different embryonic time-points, the onset of this phenotype was found to begin around E15.5 (Figure 4c). At E12.5, the NC:C ratio could not be determined as the compaction process has not yet begun and trabeculation is very abundant in all genotypes. At this stage, the ventricular wall thickness was not significantly different compared to wildtype. At E14.5, when compaction has just begun, the NC:C ratio was not elevated in *Irx4*KO mice. However, by E15.5, the NC:C ratio is noticeably higher in *Irx4*KO mice, with a NC:C ratio of 1.42 in the mutant versus a ratio of 1.24 in wildtype. The difference is further enlarged by P0, where the NC:C ratio is 1.65 in *Irx4*KO mice versus 1.02 in wildtype. While displaying this positive trend, it is important to note that none of the measurements are statistically significant.

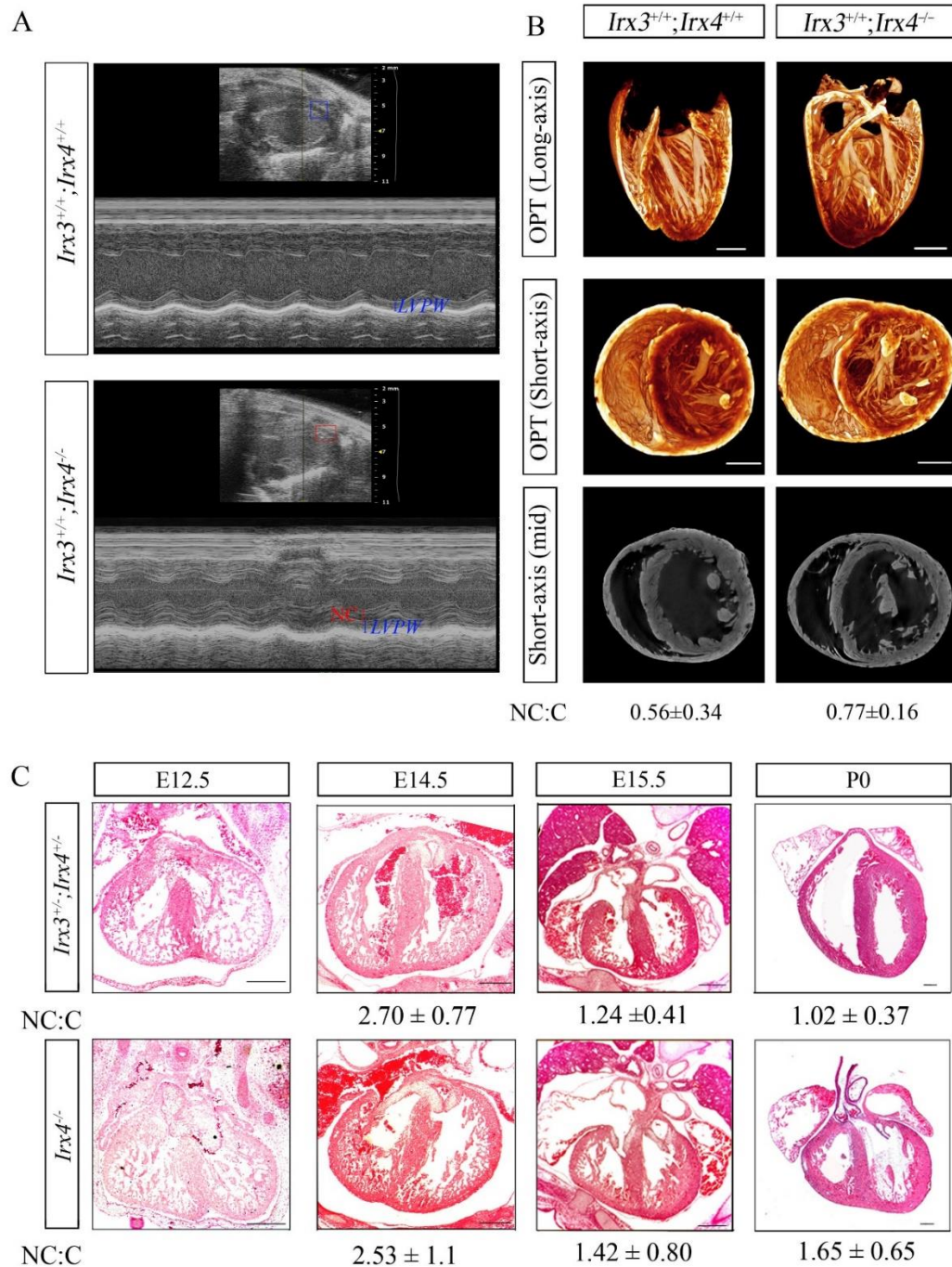


Figure 4. *Irx4*KO mice have a mild noncompaction phenotype. A) Echocardiography consistently show increased trabecular projections in the left ventricular chamber in comparison to the double-heterozygous control (n=6). Noncompacted region (NC) was boxed and labeled in red. B) Optical Projection Tomography also show increased trabeculation at the apical level and papillary muscles farther from the ventricular wall (n=3). C) Histology across embryonic time points display the development of noncompaction phenotype by E15.5.

3.2 *Irx3^{+/-};Irx4^{-/-}* and *Irx3;Irx4*DKO mutants exhibit ventricular noncompaction

3.2.1 Mutant hearts with a functional copy of *Irx4* are phenotypically normal

Since breeding of *Irx3^{+/-};Irx4^{+/-}* mice results in double KO and wildtype mice, each being born at a probability of 1/16, it is very rare for both genotypes to occur in the same litter. In order to obtain a littermate control for analysis, it was necessary to establish if *Irx3^{+/-};Irx4^{+/-}* mice are phenotypically identical to wildtype mice. All visualization techniques, including histology, OPT, and echocardiography, revealed very similar structures without any abnormal development (Figure 5). Therefore, in all my phenotypic analyses, *Irx3^{+/-};Irx4^{+/-}* mice were used as the littermate control.

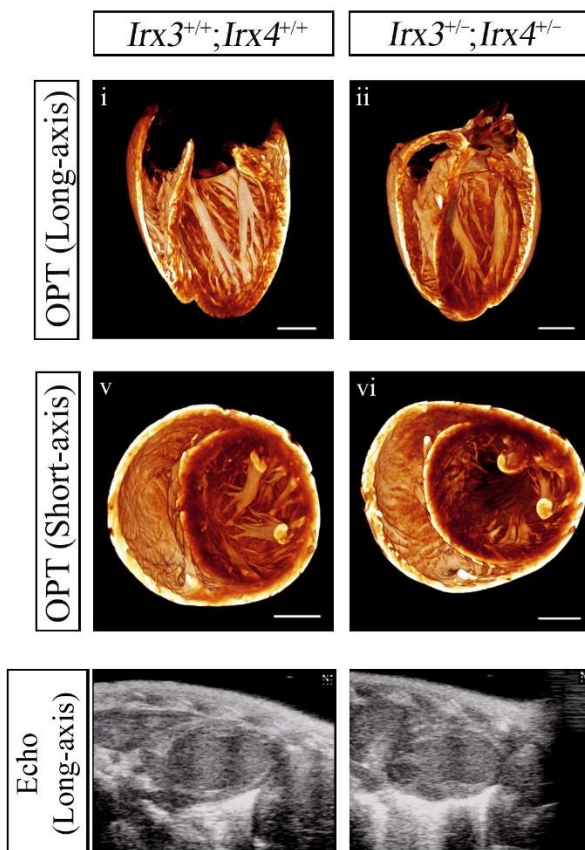


Figure 5. *Irx3^{+/-};Irx4^{+/-}* mutants have a normal phenotype comparable to the wildtype. In both OPT and echocardiography, morphology was normal in the double-heterozygotes, making it a suitable control.

As well, $Irx3^{-/-}$ and $Irx3^{-/-};Irx4^{+/-}$ hearts showed adequate myocardial compaction and did not exhibit any abnormal muscle structures (Figure 6). Specifically, OPT data depicted two normal and discrete papillary muscles as well as compact wall structures. In summary, my analysis revealed that all genotypes with a functional copy of $Irx4$ undergo a typical compaction process.

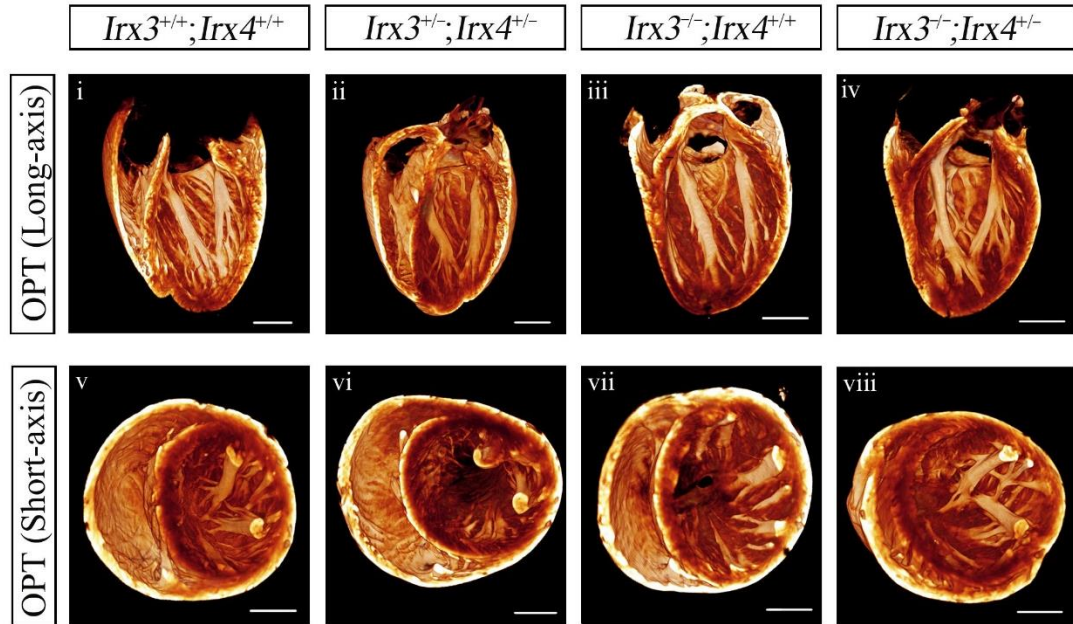


Figure 6. All mutants with a functional copy of $Irx4$ have normal morphology. WT, double-heterozygotes, $Irx3^{+/-};Irx4^{+/-}$ and $Irx3^{-/-};Irx4^{+/-}$ mutants have normally compacted ventricular wall and normal papillary muscle structure and placement.

3.2.2 $Irx3;Irx4$ DKO mutants exhibit a partial postnatal lethality

First, the viability of the double mutants had to be addressed. While both single KO mice, as previously stated, were viable and fertile, preliminary data by Dr. Bruneau's group had suggested that the DKO mice were embryonic lethal. Therefore, careful management was done to determine ratio of mutants born and their general health.

$Irx3;Irx4$ DKO mice are viable as they are born at a normal Mendelian ratio. However, more than three quarters of $Irx3;Irx4$ DKO mice die before P21 (Figure 7) and display a significantly lower body weight compared to their littermates (Figure 8a). Their smaller size appears to be due to developmental delay rather than thinness, with features such as head and ear structures of early neonatal pups (Figure 8b). Due to this postnatal lethality and cardiac wasting syndrome, most

phenotyping efforts were concentrated at P14, when the majority of the DKO mice were alive, and further studies were performed at 5 weeks on the surviving mutants to observe the adult phenotype.

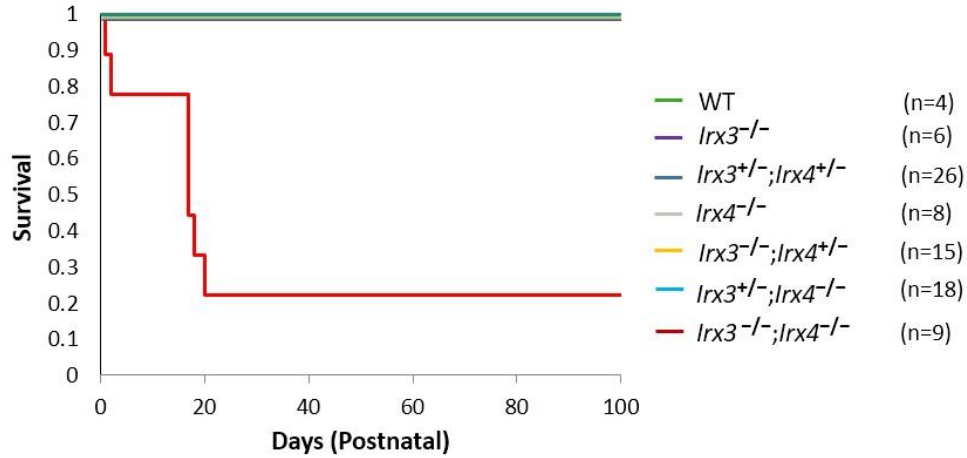


Figure 7. *Irx3*;*Irx4*DKO mutants show a partial postnatal lethality. More than 75% of the double mutants die before weaning age. Surviving double-mutants live a normal lifespan.

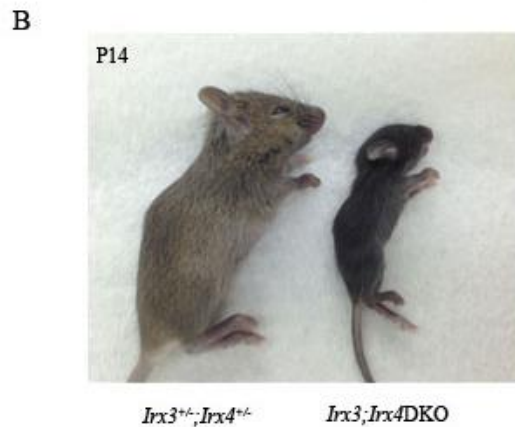
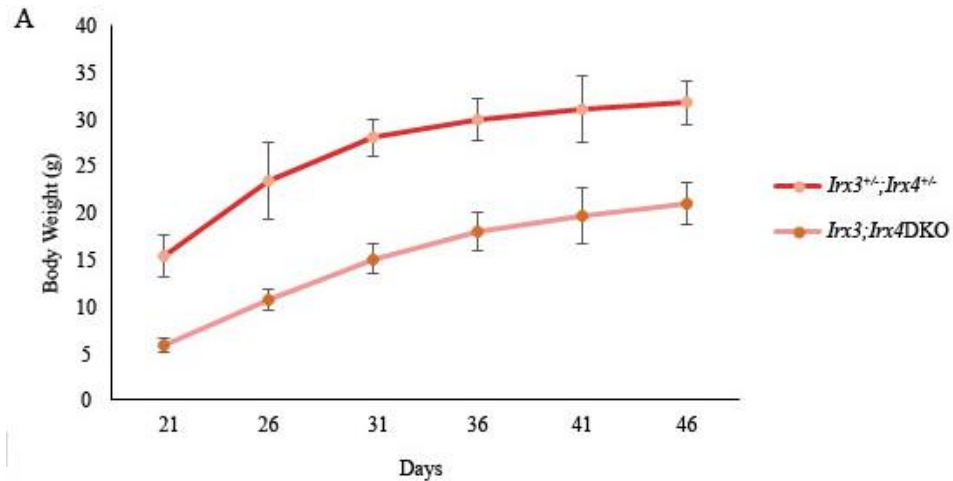


Figure 8. *Irx3;Irx4*DKO mice show a cardiac wasting phenotype. A) They consistently have a lower body weight throughout its life time in comparison to other genotypes. B) Double knockouts show developmental delays and an inability to gain weight.

3.2.3 Additional loss of *Irx3* exacerbates the noncompaction phenotype of *Irx4*KO mice in a dose-dependent manner

When *Irx3* is deleted in the *Irx4*KO background, a more severe noncompaction phenotype begins to emerge (Figure 9). In comparison to the mild noncompaction phenotype seen in *Irx4*KO mice, *Irx3^{+/-};Irx4^{-/-}* mice no longer possess two discrete papillary muscles, instead the mutant ventricular chambers contain many projections and nodes. Though statistically insignificant, the NC:C ratio of *Irx3^{+/-};Irx4^{-/-}* hearts is increased by 2-fold when compared to the *Irx3^{+/-};Irx4^{+/-}* control (Figure 9). *Irx3;Irx4*DKO mice display the largest increase in noncompact trabeculation with a significantly higher ratio of 1.95 ± 0.35 , almost four times the value of the *Irx3^{+/-};Irx4^{+/-}* control. Their noncompaction starts near the base of the heart reaching the tip of the apex. Interestingly, these projections and muscle branches also appear to connect with each other with thick structures of a lower density, as denoted by the darker and transparent coloring.

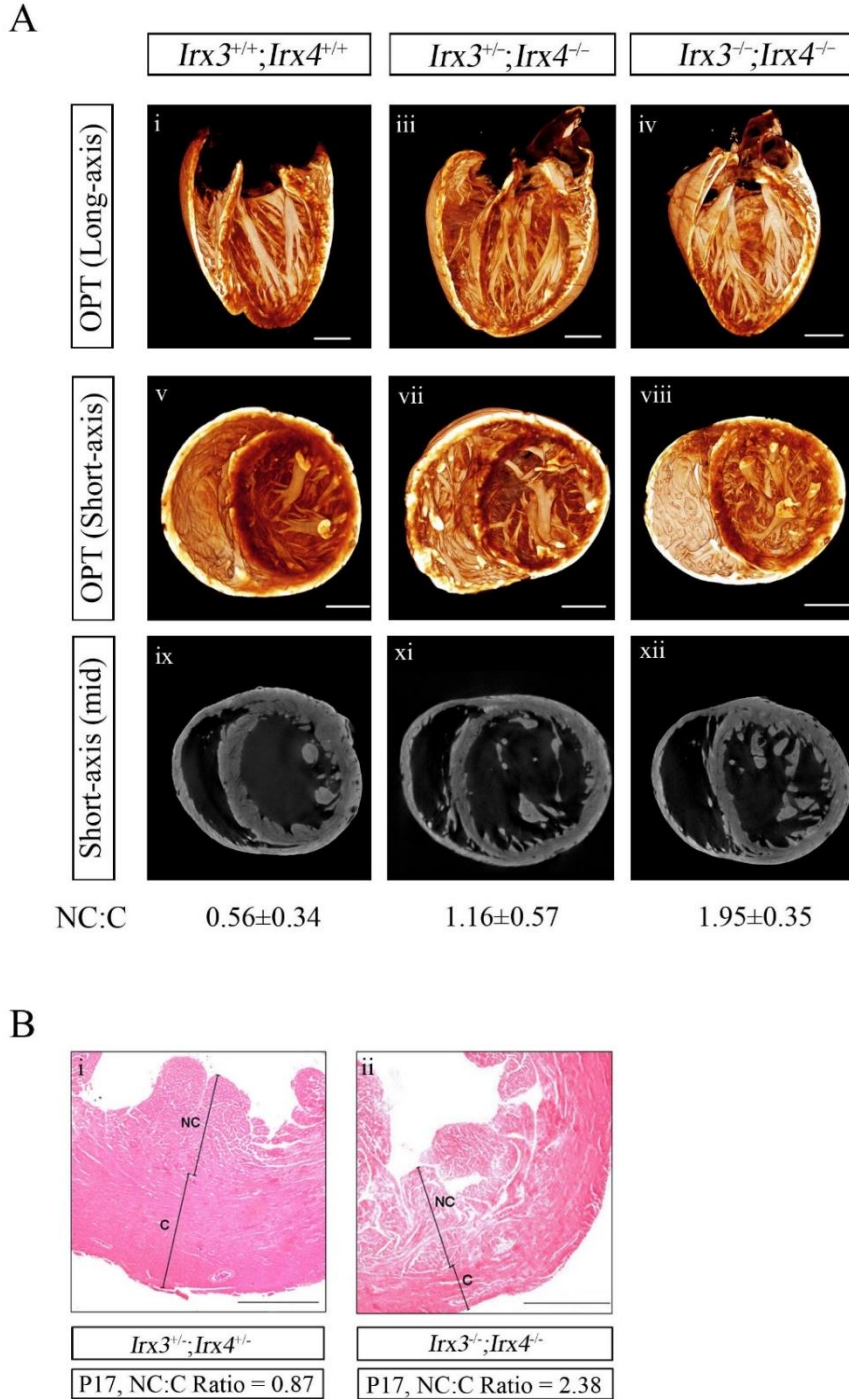


Figure 9. Dose-dependent loss of *Irx3* in an *Irx4*KO background increase noncompaction severity. A) *Irx3^{+/-};Irx4^{-/-}* show increased trabeculation and disrupted papillary muscle structure. Trabeculation begins near the base and papillary muscles are no longer two discrete bundles. *Irx3;Irx4*DKO show highest level of noncompaction beginning at the base, display disrupted papillary muscle structure, and regions of thin ventricular wall. B) Histology confirmed this increase in trabeculation in the double-knockouts.

Histological analysis of *Irx3;Irx4*DKO mice at time of death (~3 weeks of age) showed similar additional muscular nodes in the ventricular chamber, noncompact trabeculation, and abnormal connection between the muscular nodes (Figure 10a-c), all of which corresponds to the OPT data. Additionally, there is an altered papillary muscle structure. What appears to be the posteromedial papillary muscle has shifted towards the septum and eventually becomes connected to the septum (Figure 10d-e). In two *Irx3;Irx4*DKO mice, there was also a ventricular septation defect close to the posterior side of the septum, or at least only a thin flap is present instead of muscle (Figure 10f).

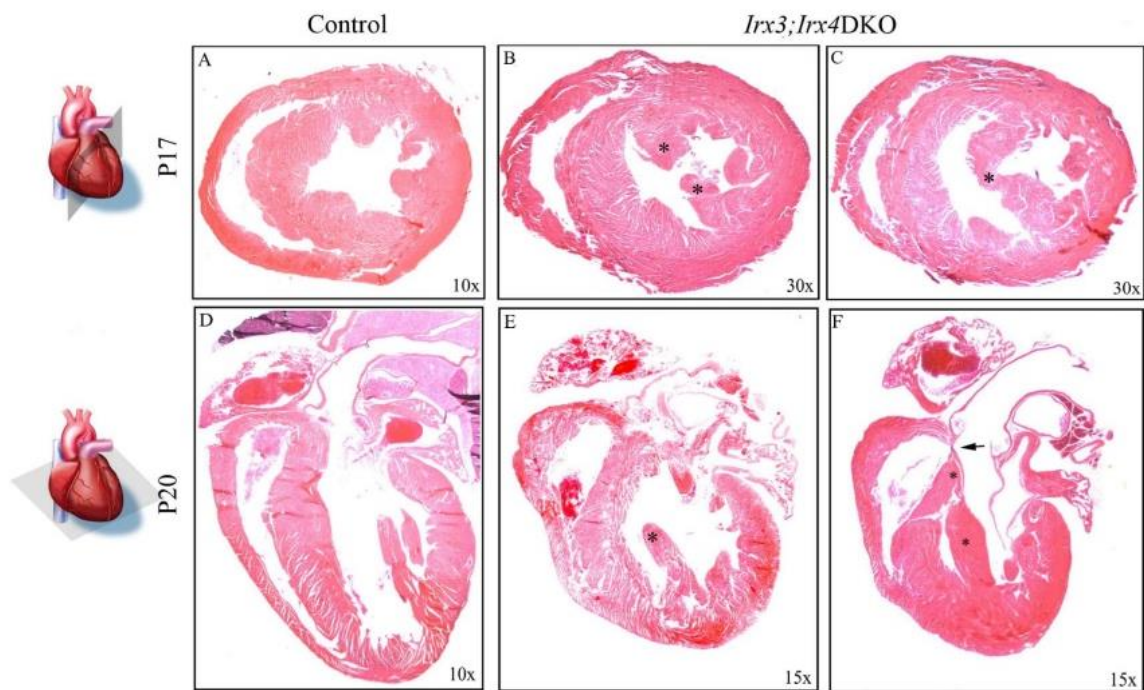


Figure 10. Abnormal trabeculation and muscle structure are present in the *Irx3;Irx4*DKO mice. Sections of double-knockout hearts near time of death show abnormal connections between additional muscle structures, thin ventricular septum at the basal region, and noncompaction.

Trichrome staining was used to determine if scarring occurred in the heart as a part of the pathology, and it was found that no fibrosis was present within the muscle structures.

Intriguingly, the interconnection between the abnormal muscular structures was found to be collagenous in nature (Figure 11a-c). The mitral valve in the *Irx3;Irx4*DKO mice also appears to

be elongated (Figure 11d-h). In addition, the much smaller papillary muscle seems to be covered by a thin layer of connective tissue (Figure 11i).

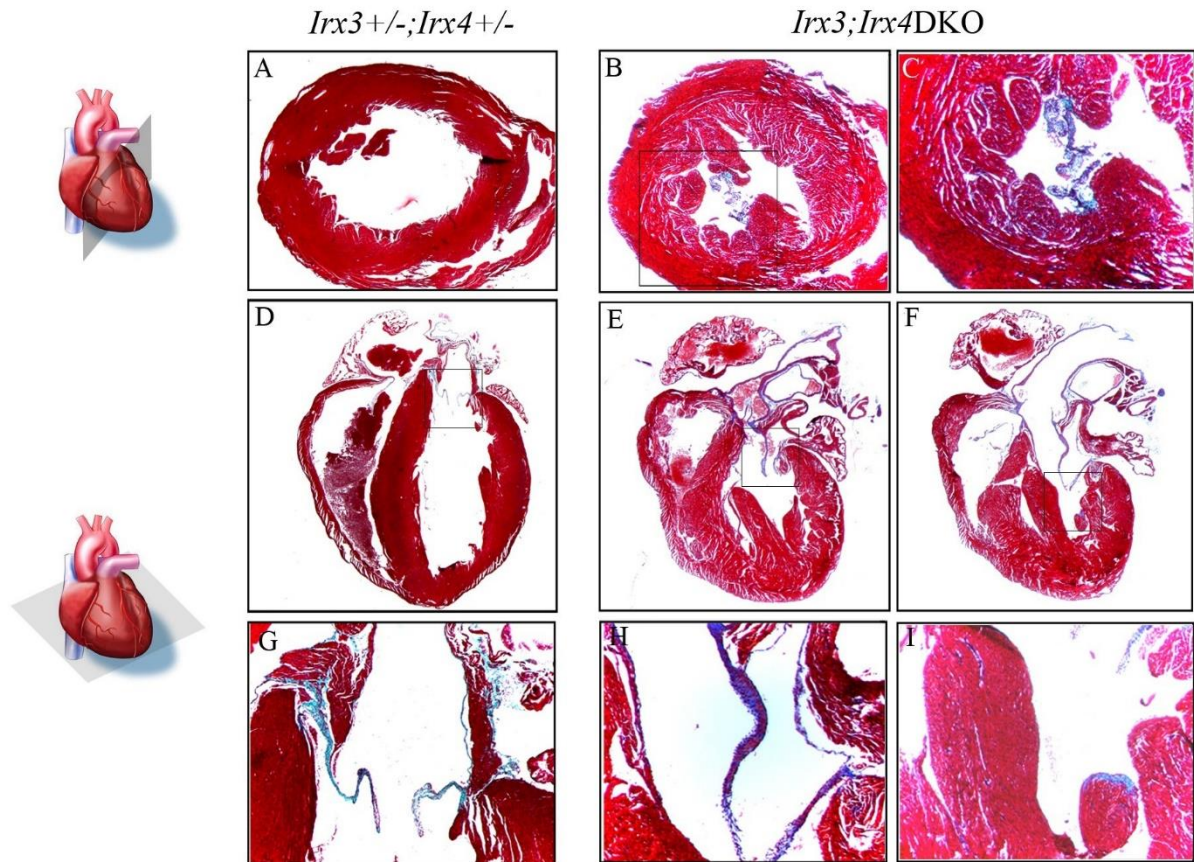


Figure 11. Double mutants have collagenous deposits between muscle structures and abnormally long mitral valves. Trichrome staining stains all collagen blue. In the double-knockout, collagenous linkages are confirmed between the muscle structures. Mitral valve is also abnormally long, connecting to a very small papillary muscle covered in a layer of connective tissue.

3.3 *Irx3;Irx4DKO* mice show systolic dysfunction and mitral regurgitation

Echocardiography, as the gold standard of human LVNC, was also utilized in these mutants to investigate the systolic and mitral functions of the heart. It was performed first on P14 samples, as most mice were still alive at this time point before weaning. Systolic functioning was measured through the ejection fraction (EF), which is the percent of blood pumped out from the

left ventricle, and fractional shortening (FS), which is the change in wall movement as the heart contracts. While there is an overall general trend of decreasing EF and FS, the values of *Irx3;Irx4*DKO mice are not significantly different from those of control mice, due to large variations between samples (Figure 12). Nonetheless, some *Irx3;Irx4*DKO mice were dramatically sicker than others.

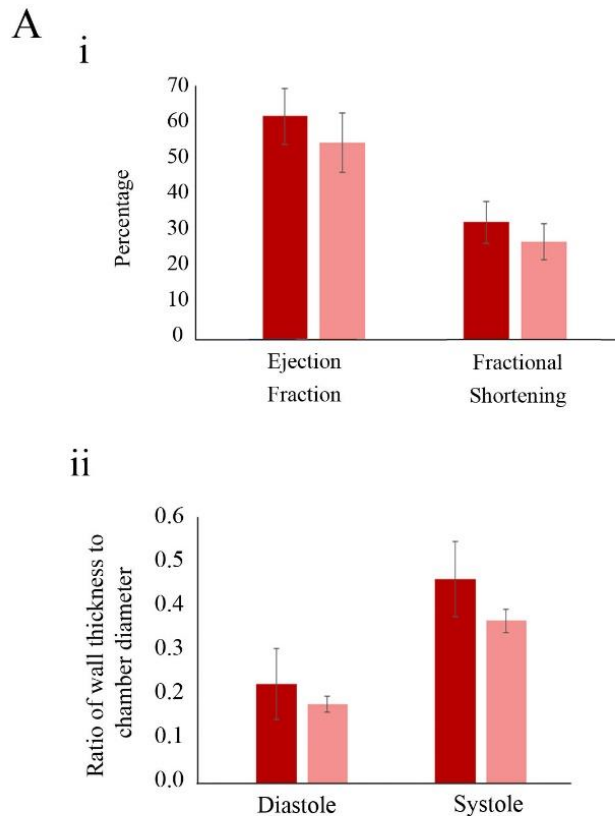


Figure 12. Echocardiography at P14 did not show significant differences in systolic function and wall thickness. A) Neither ejection fraction nor fractional shortening were significantly decreased in the double-knockouts. B) Wall thickness as normalized to left ventricular diameter is decreased but not significantly so. (n=3).

Another parameter I measured is mitral valve functioning. As the papillary muscle and underlying heart wall structure were altered in the *Irx3^{+/-};Irx4^{-/-}* and *Irx3;Irx4*DKO mice, it was reasonable to hypothesize that the mitral valve, which is closed during systole to prevent the backflow of blood into the left atrium, may not be able to withstand the high pressure at systole due to the disrupted support, allowing for regurgitant jets. However, Colour Doppler Mode Echocardiography did not observe any mitral regurgitation in these mutant mice at P14.

Unlike the analysis at P14, echocardiography at 5 weeks of age detected significant systolic and diastolic dysfunction (Figure 13A). Ejection fraction was lowered significantly by 7.16% and fractional shortening by 5.28% in *Irx3;Irx4*DKO mice compared to *Irx3^{+/-};Irx4^{+/-}* mice (Figure 13Ai). The left ventricular wall thickness as normalized to the left ventricular chamber diameter was not significantly decreased during diastole but significantly decreased during systole as muscles contract (Figure 13Aii). The heart weight to body weight ratio is used as a sign for hypertrophic cardiomyopathy, and will be increased in hypertrophic cases as the heart enlarges. This ratio was not significantly altered in *Irx3;Irx4*DKO mice suggesting that hypertrophy is not present at 5 weeks (Figure 13Aiii).

Mitral functioning of *Irx3;Irx4*DKO mice was noticeably reduced at 5 weeks. First, mitral regurgitation was noted in 3 out of 5 *Irx3;Irx4*DKO mice observed after weaning age. The severity of the regurgitation varied by sample, but was generally mild, with a small separate jet following contractile motion into the left atrium. There was an increase in mitral valve deceleration time, which is a measure of how fast the valve closes and an indication of the flexibility or stenotic quality of the mitral valve. There was also an insignificant trend of increasing E/A ratios (Figure 13Aiv), which have been linked to diastolic dysfunction and mitral regurgitation severity⁵⁷.

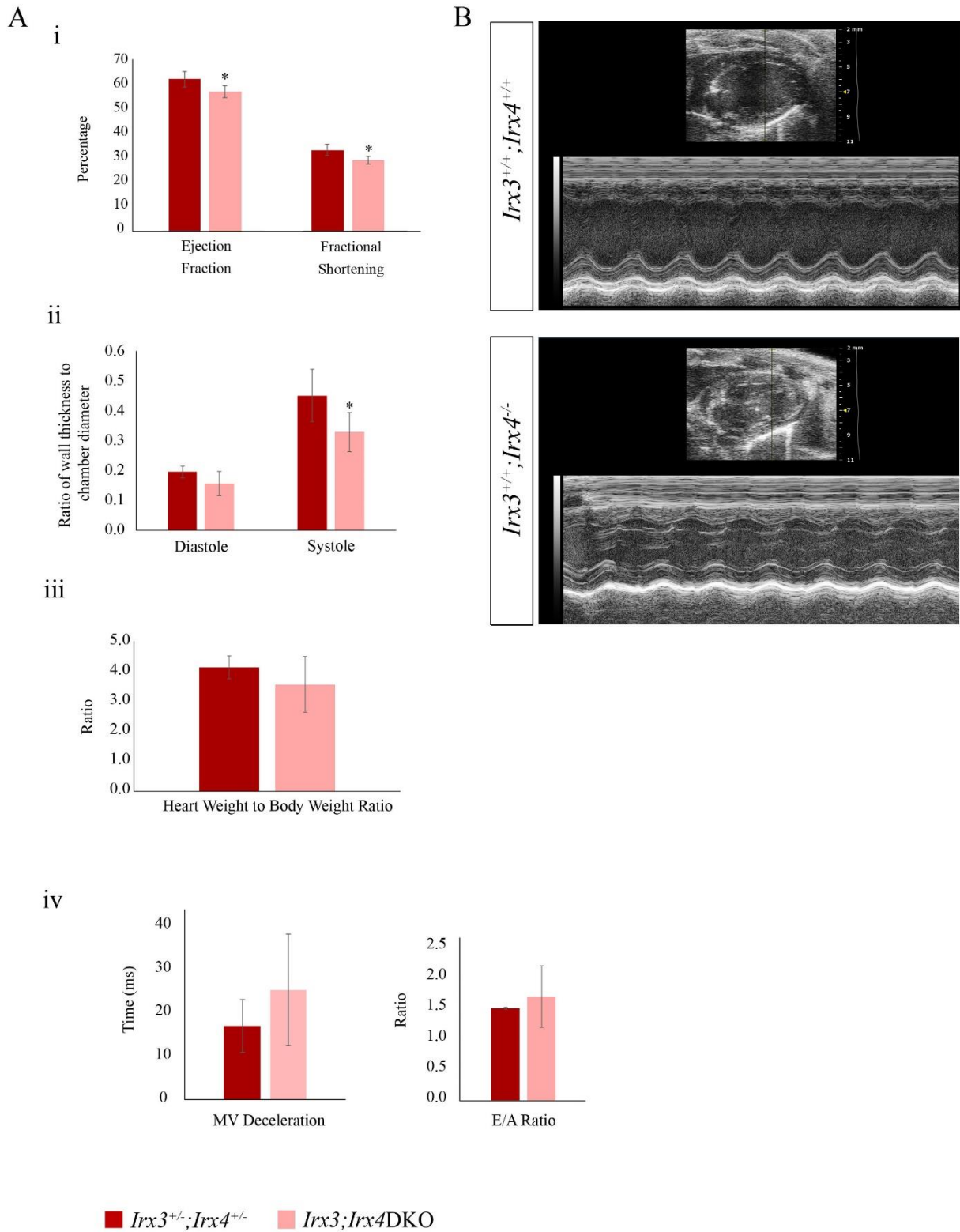


Figure 13. Echocardiography at 5 weeks of age show significant changes in heart function.

Ai) Contractile function is significantly decreased in double-knockouts in both ejection fraction and fractional shortening. Aii) Wall thickness normalized to left ventricular chamber diameter

was also significantly decreased during systole and nonsignificantly decreased in diastole. Aiii) Heart weight to body weight ratio was not significantly altered in the double-knockouts. Aiv) Mitral valve function shows a positive trend to dysfunction but not significantly so. B) Echocardiography at 5 weeks show noticeably different contractility and higher trabeculation. (n=4, *p < 0.05).

3.4 *Irx3;Irx4*DKO mice show elevated expression of heart failure markers

Expression of heart failure marker genes is used to indicate heart failure in the mutant mice. Ventricular cardiac tissue was taken in mice at 5 weeks because while they have survived the neonatal period, their hearts have been stressed for a longer period of time. As the samples are not from blood, we expect to detect moderate elevations between 2 to 10-fold. Five weeks old *Irx3;Irx4*DKO mice show significantly higher expression of heart failure marker genes. They exhibit a 9.4-fold increase in *Nppa* mRNA expression, 3.2-fold increase in *Acta1*, and 2.5-fold increase in *Nppb* (Figure 14).

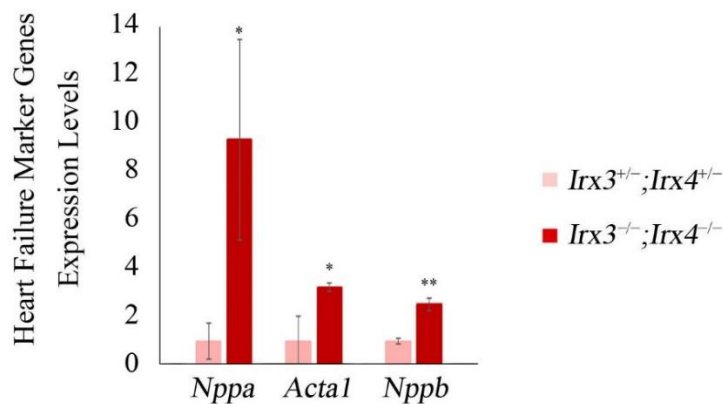


Figure 14. Heart failure markers are increased at 5 weeks in the *Irx3;Irx4*DKO heart. Heart failure markers *Nppa*, *Acta1*, and *Nppb* were quantified by RT-qPCR. (n=3, *p < 0.05, **p < 0.01).

3.5 Mutant mice exhibit myocardial and patterning changes at E14.5

3.5.1 *Irx3;Irx4*DKO mutants show thinner ventricular wall by E14.5

To investigate whether *Irx3;Irx4*DKO mice exhibit an embryonic heart phenotype, I examined mutant and control mice at E14.5. The ventricular wall of E14.5 *Irx3;Irx4*DKO mice was significantly thinner (67%) when compared with those of the control mice, though the area of trabeculation appeared unaffected (Figure 15).

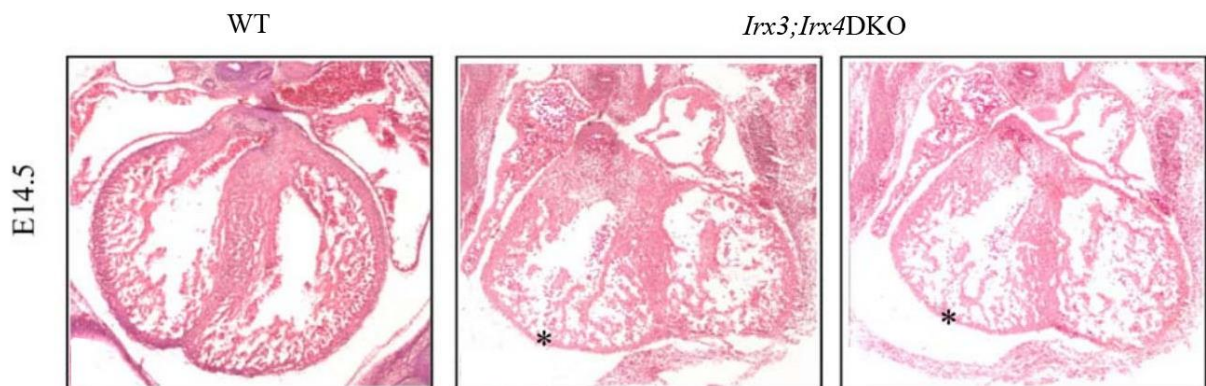


Figure 15. Ventricular wall is significantly thinner at E14.5 in *Irx3;Irx4*DKO samples.

Histology of double mutant hearts display less compact trabeculae and thinner ventricular wall.

3.6 *Irx3;Irx4*DKO hearts have increased PECAM-positive endocardial cells, higher expression of trabecular markers, and a thinner layer of compact marker

To confirm these findings, *in situ* hybridization using appropriate markers for the different layers of myocardium was performed at E14.5 to determine whether there is a change in the composition of the tissue layers. This analysis revealed an expansion in the expression domain of the trabecular marker *Nppa*, which marks the noncompact trabeculae in *Irx3;Irx4*DKO mice (Figure 16a). In addition, *Irx3;Irx4*DKO hearts showed reduced expression of the myocardium marker *Tbx20* suggesting a decreased compaction of the heart wall. While the myocardial marker *cTnI* was detected throughout the myocardium including the trabecular regions of both *Irx3^{+/-};Irx4^{+/-}* and *Irx3;Irx4*DKO mice, the expression domain of the endocardial marker *Pecam* appeared thicker in *Irx3;Irx4*DKO mice than the control at the trabecular base (Figure 16b).

These results suggest that E14.5 *Irx3;Irx4*DKO hearts show signs of reduced compaction with increased noncompact trabeculae and an expanded endocardial layer.

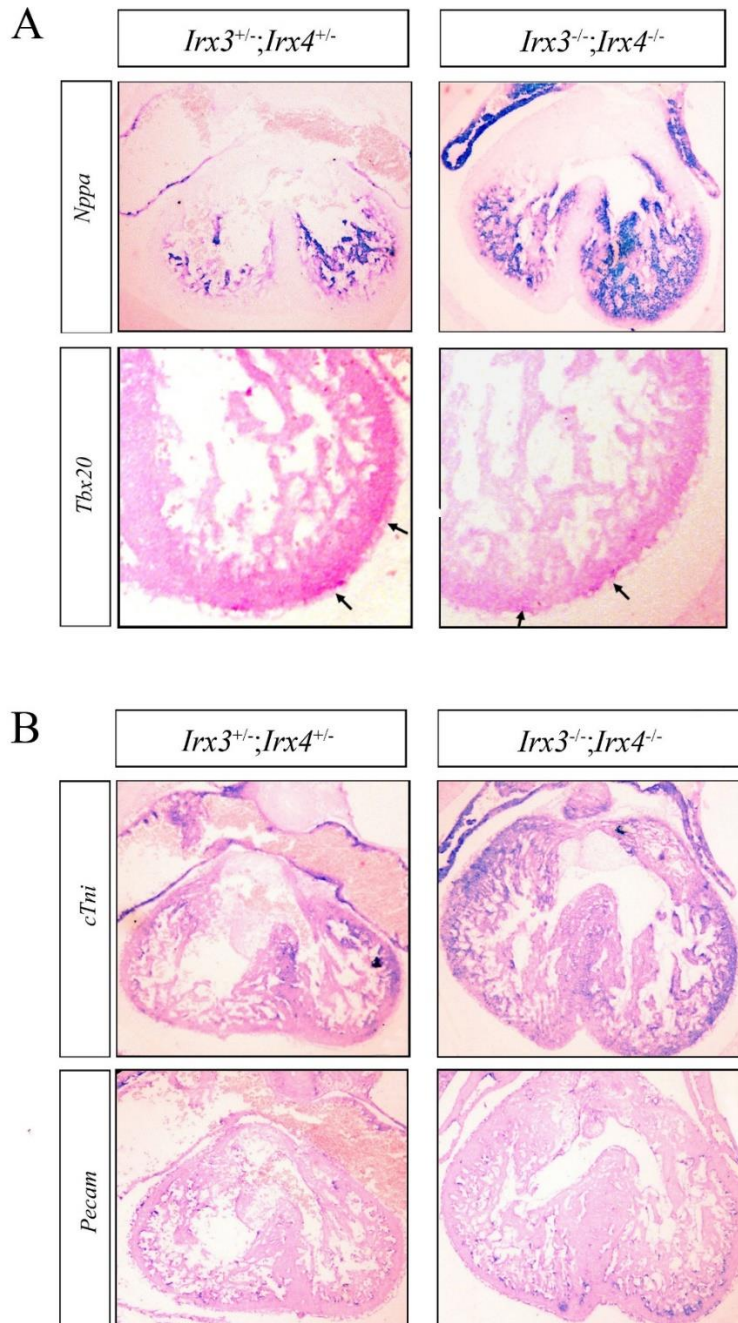


Figure 16. *Irx3;Irx4*DKO mice have expanded trabecular marker expression domain and a thickened endocardial layer. A) Trabecular marker *Nppa* is increased throughout the noncompact trabecular regions, into the compacted ventricular wall. Compact myocardium marker *Tbx20* show reduced expression in the double-knockouts. B) *cTni* marks myocardial cells and shows normal myocardial identity throughout the ventricles of both genotypes.

Endocardial marker *Pecam* shows a thicker layer of endocardial cells at the base of the trabecular region of the double-knockouts.

3.7 Changes in molecular pathway are found in *Irx3;Irx4* mutants at E14.5 when compaction begins

As E14.5 marks the beginning of the compaction process, associated pathway changes are anticipated to occur near this time-point. RT-qPCR was used to determine mRNA-level changes in genes associated with the LVNC phenotype and *Irx* family genes.

3.7.1 *Irx5* is upregulated in the LVNC mutants

To further explore the endocardial phenotype of *Irx3;Irx4*DKO mice, I examined the expression of *Irx5*, which is a marker of endocardial cells. RT-qPCR analysis revealed that *Irx5* expression is up-regulated in E14.5 *Irx3^{+/-};Irx4^{-/-}* (2.1-fold) and *Irx3;Irx4*DKO (3.1-fold) hearts (Figure 17a). At P21, *Irx3^{+/-};Irx4^{-/-}* hearts showed a significant increase (2.3-fold) of *Irx5* expression (Figure 17b). These results are consistent with an expansion of the endocardial layer in the *Irx3;Irx4* mutant hearts.

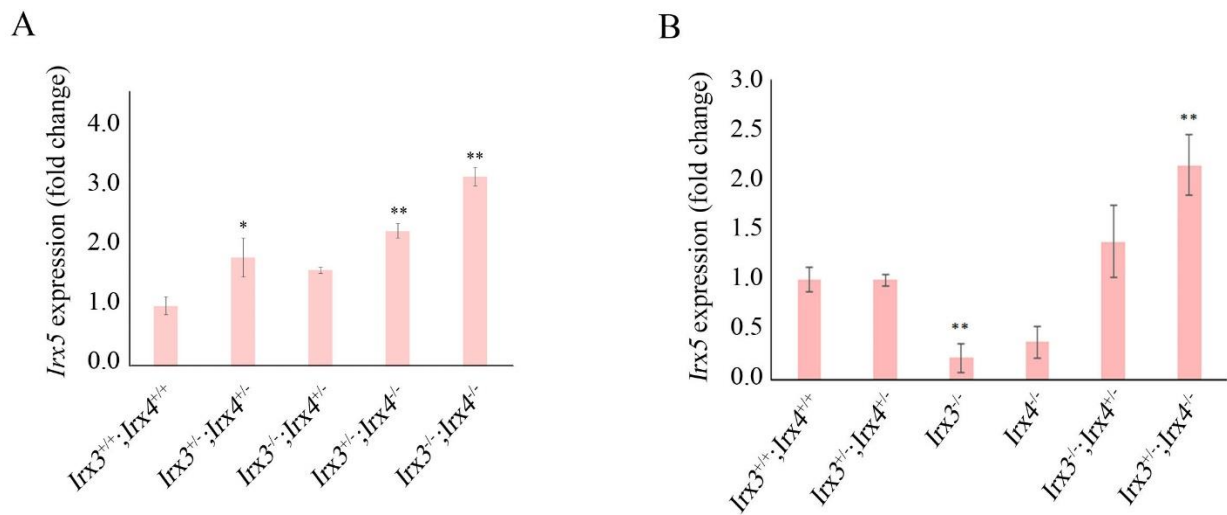


Figure 17. There is maintained upregulation of *Irx5* in *Irx3;Irx4*DKO mutants. A) At E14.5 and B) P21, *Irx5* expression is increased slightly in the *Irx3^{+/-};Irx4^{-/-}* and significantly in the *Irx3;Irx4*DKO. n=3 per genotype, * p<0.05, ** p<0.01.

3.7.2 *Irx3;Irx4* mutants have altered Bmp10 expression

Bmp10 pathway, with its numerous implication in LVNC mouse models and regulation by IRX3, was the obvious choice in a selective approach in determining pathway changes.

3.7.2.1 *Bmp10* gene is upregulated in many double mutants, but downstream target genes are only altered in mutants with noncompaction

At E14.5, *Bmp10* is upregulated 3.2-fold (± 0.02) in DKO mice and 2.8-fold (± 0.04) in *Irx3*^{-/-}; *Irx4*^{+/-} mice (Figure 18a). *Bmp10* target genes implicated in noncompaction are also affected.

Upstream of *Bmp10*, *Notch1* as an output of Notch signaling is increased similarly in the double mutants, with the highest at a 2.5-fold (± 0.048) increase in the DKO mice (Figure 18b). *Tbx20*, a downstream target gene of *Bmp10* pathway is significantly up-regulated in the DKO mice at a 2.2-fold (± 0.22) increase (Figure 18c).

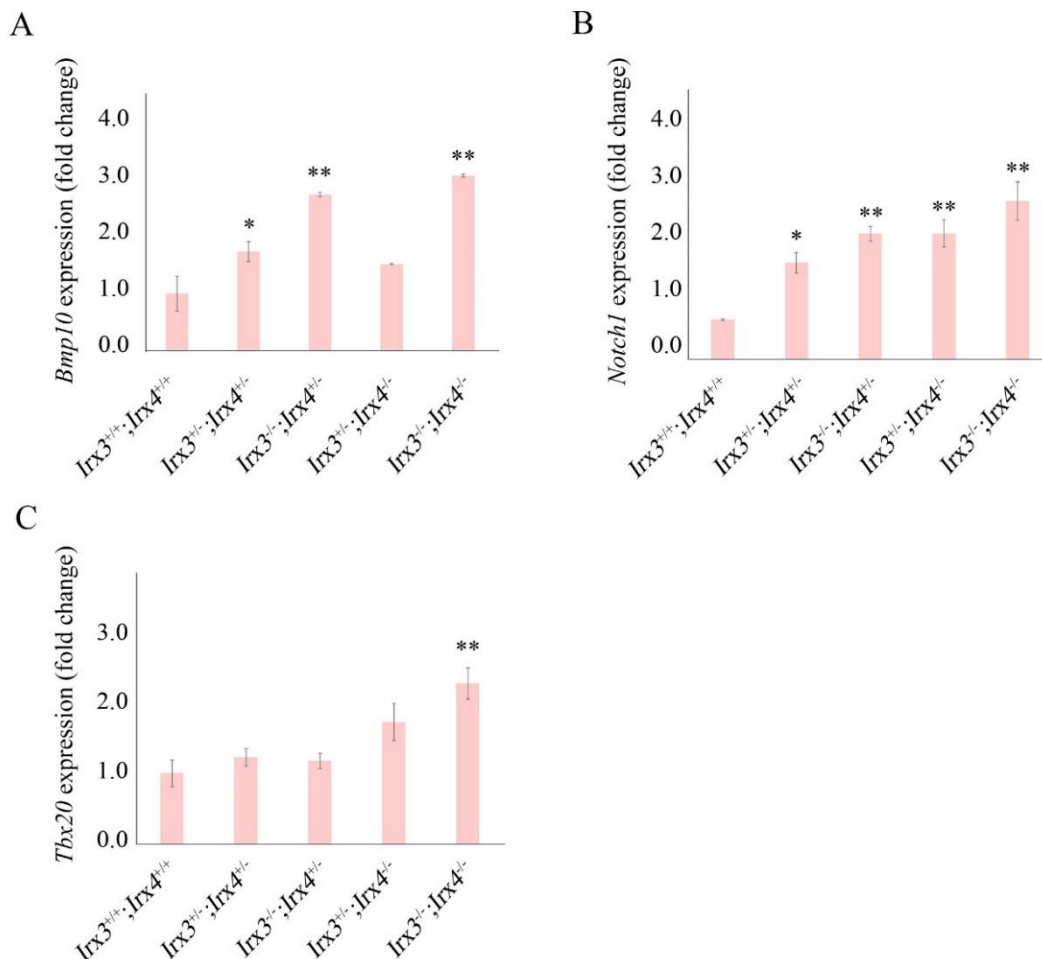


Figure 18. There is upregulation of Bmp10 pathway genes at E14.5. A) *Bmp10* is increased in the double mutants. B) Correspondingly, upstream Notch pathway is also upregulated throughout the double mutants. C) Downstream target gene *Tbx20* is only significantly upregulated in the *Irx3;Irx4*DKO samples. n=3 per genotype, * p<0.05, ** p<0.01.

As mouse models of LVNC with increased Bmp10 pathway activation have increased cardiomyocyte proliferation, the next step was also to determine if cell proliferation is altered in the *Irx3;Irx4* mouse mutants.

Proliferation pattern was observed using immunofluorescence of phospho-histone H3 (PH3) staining. PH3-positive cells were counted at different levels of the ventricular heart wall, labelled as Basal, Mid-Basal, Mid, and Apical regions (Figure 19a). Compared to published proliferation patterns at E13.5, the DKO mutant hearts have a significantly increased rate of proliferation in the Mid-basal and Apical regions of the left ventricular wall (Figure 19b-c). While wildtype heart has a relatively higher rate of proliferation in the mid-region, DKO mutant hearts display higher cell proliferation throughout the entire lateral wall.

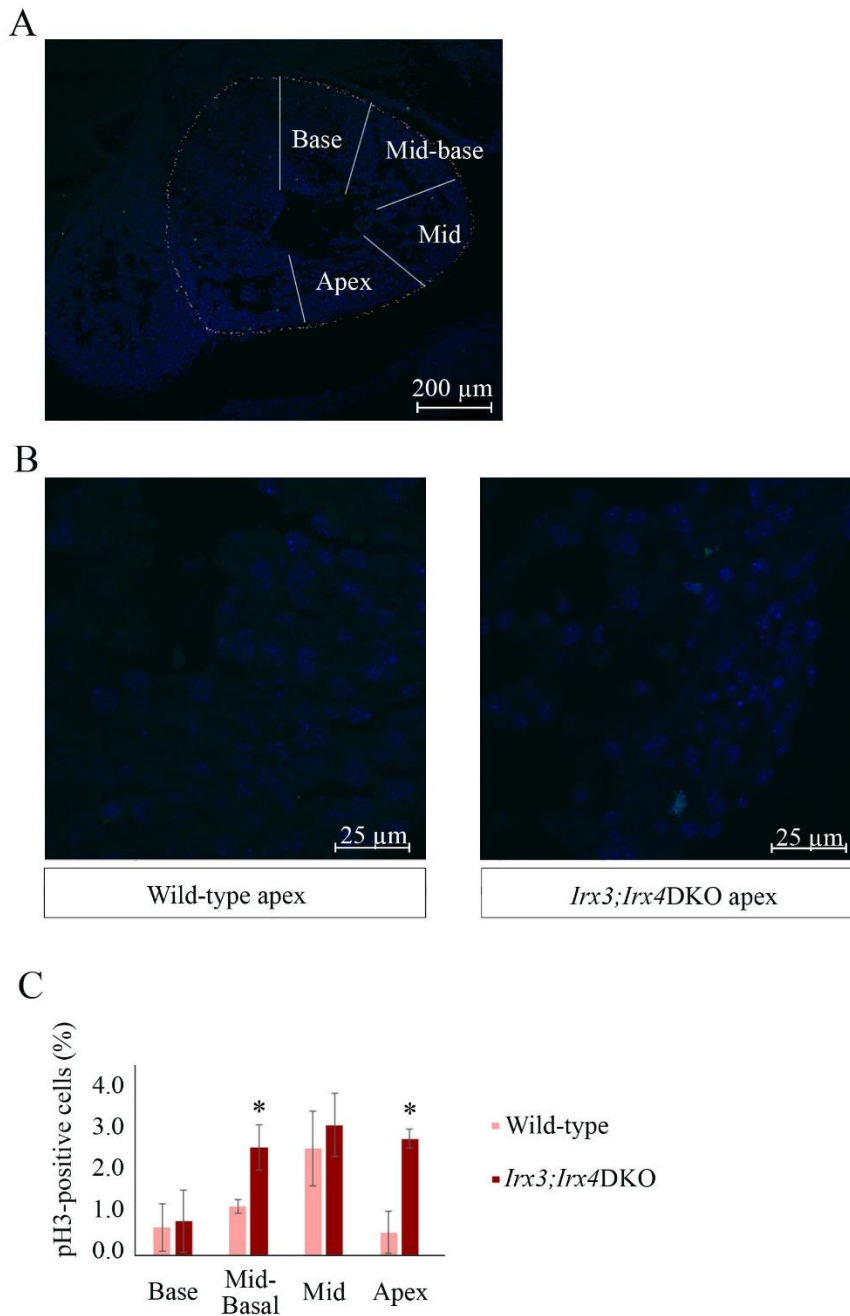
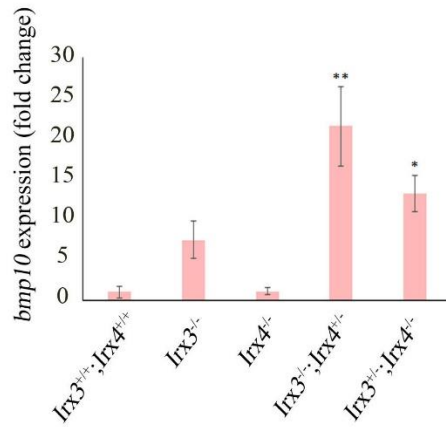


Figure 19. Immunofluorescence analysis of mitotic marker phospho-histone H3 show increased cell proliferation in the left ventricular free wall of the *Irx3;Irx4DKO* mice. A) E13.5 hearts were divided into four regions to be imaged. B) Images were taken using confocal microscopy and the pH3-positive cells were counted. C) There is significantly increased percentage of proliferative cells in the double knockouts in the Mid-basal and Apical area.

At P21, *Bmp10* upregulation is found in the *Irx3*^{-/-}, *Irx3*^{-/-};*Irx4*^{+/-}, and *Irx3*^{+/-};*Irx4*^{-/-} mutant hearts (Figure 20a). As Bmp10 signals through the nuclear translocation of pSMAD1/5/8 effectors, immunofluorescence of nuclear pSMAD1/5/8 was performed to investigate whether the Bmp10 pathway is activated in these mutant hearts. In *Irx4*KO hearts, which showed low *Bmp10* mRNA expression, nuclear pSMAD1/5/8 signals were barely detectable (Fig. 20b). Conversely, *Irx3*^{+/-};*Irx4*^{-/-} hearts, which exhibited highly elevated expression of *Bmp10*, displayed strong nuclear staining of pSMAD1/5/8, indicating that the noncompaction phenotype indeed involves a robust activation of the Bmp10 pathway. In contrast, although *Bmp10* expression was elevated in *Irx3*^{-/-};*Irx4*^{+/-} hearts (which did not have a noncompaction phenotype), there was no downstream activation of the pathway as revealed by little or no nuclear localization of pSMAD1/5/8. These results suggest that *Bmp10* up-regulation *per se* is not sufficient to drive a noncompaction phenotype.

A



B

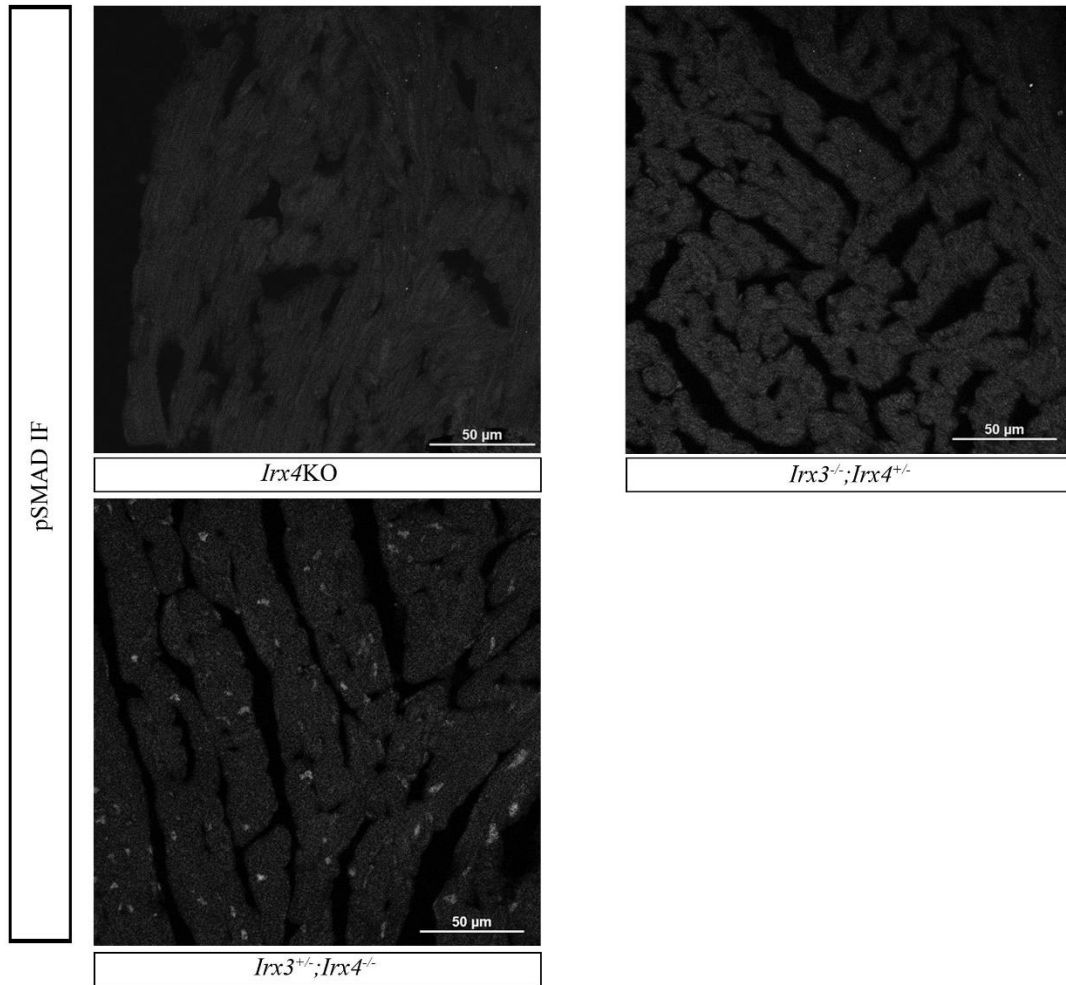


Figure 20. *Bmp10* expression is upregulated at P21 but pathway activation only occurs in the absence of IRX4. A) P21 Rt-qPCR show upregulated *Bmp10* expression in the *Irx3^{+/-};Irx4^{-/-}*

as well as the *Irx3*^{-/-};*Irx4*^{+/-} mutants. B) Downstream pathway activation by the pSMAD1/5/8 phosphorylation and translocation to the nucleus was not seen in the *Irx3*^{-/-};*Irx4*^{+/-} mutants, only in the *Irx3*^{+/-};*Irx4*^{-/-} mutants.

Chapter 4 . Discussion

4 Discussion

4.1 Loss of *Irx3* exacerbates the noncompaction phenotype of *Irx4*KO mice

Previously, it was reported that *Irx4*KO mice develop cardiac hypertrophy in adulthood without congenital cardiac malformations as observed using echocardiography⁵³. The analysis presented here clearly revealed a subtle compaction defect in *Irx4*KO mice. We utilized both histology and OPT since echocardiography, which was the sole technique used in the previous study of the *Irx4*KO heart phenotype⁵³, has limited resolution and structures are constantly masked by the moving heart. Together, our analysis illustrates the presence of unresolved trabeculation and muscle branches at the base of the papillary muscles. During embryonic heart development, the ratio of noncompact trabeculation in comparison to the control only began to differ at E15.5, suggesting either an earlier arrest or overall slower progress in the compaction process. Nonetheless, the increased NC:C ratio of *Irx4*KO mice is not significant enough to meet the human diagnostic criteria of noncompaction²⁷. Thus, while *Irx4*KO hearts do show increased trabeculation, their phenotype is too mild to be described as LVNC.

*Irx3*KO mice do not exhibit any morphological heart abnormality. In fact, we found that any *Irx3*;*Irx4* mutant mice with a functional copy of *Irx4* have a morphologically normal heart, suggesting that *Irx4* plays a key role in not only regulating ventricular identity, but also heart wall compaction. In contrast, both *Irx3*^{+/-};*Irx4*^{-/-} and *Irx3*;*Irx4*DKO mice show greatly exacerbated heart defects mimicking human LVNC, with *Irx3*;*Irx4*DKO mice having the most severe phenotype. These observations point to a dose-dependent effect of *Irx3* in compensating for the functions of IRX4 during heart development. However, preliminary data suggest that even though both transcription factors were detected in the nuclear compartment prior to P2, co-immunoprecipitation experiments could not detect their complex formation, suggesting that they may not function together as protein complexes (Figure 21a). On the other hand, the presence of IRX3 in the cytoplasmic compartment, at moderate levels even before P2, does indicate that there may be alternative, non-transcriptional functions of IRX3 (Figure 21b).

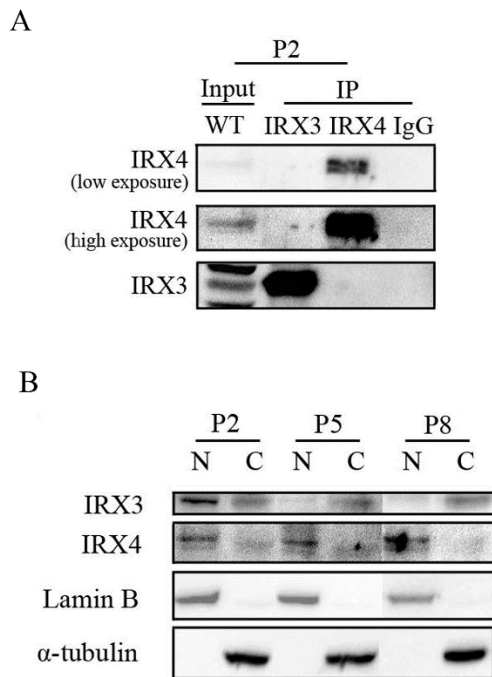


Figure 21. IRX3 and IRX4 remain in the nucleus together prior to P5, but do not appear to bind each other. A) Co-IP experiments did not detect physical interactions between IRX3 and IRX4 at P2. B) Fractionation show IRX3 switches expression domain from nuclear to mainly cytoplasmic by P5, while IRX4 does not change expression pattern neonatally.

Further quantification of noncompaction through the NC:C ratio showed an average ratio of 1.95 in *Irx3;Irx4*DKO mice, which does not exceed the human diagnostic criteria of LVNC. However, different from clinical diagnosis, which typically measures only the noncompact regions²⁴, three different levels of the heart was used in our studies to calculate the ratio for the mutants. In actuality, there are many noncompact regions in these double mutant hearts that would more than satisfy the criteria used for echocardiography and cardiac MRI²⁶.

Histological analysis revealed abnormal collagenous connection between the muscular bundles, which are also present in many cases of human LVNC²⁹. Furthermore, the OPT data illustrated many connective tissues that are not as dense as muscles, resembling valve tissue instead. The exact cause of these abnormal connecting tissues is unknown. While one study has suggested insufficient blood flow to these extensive regions as a cause for these tissues⁶⁵, histology of the *Irx3;Irx4*DKO samples and many human samples in the published literature indicates that they

appear as additional linkages between muscles rather than necrotic areas within a muscle. The presence of these collagenous tissues may indicate a defect in the delamination process forming the papillary muscles and chordae tendineae attachments¹³, perhaps disrupted by the same cause as noncompaction.

Another morphologic change is the presence of a thicker layer of endocardial cells in the *Irx3;Irx4*DKO hearts. The process by which this occurs is unknown, but an expansion of the endocardial layer may be involved in the growth of the trabecular layer in the mutants, as secreted factors from the endocardial layer, such as NOTCH ligands, are required to induce trabecular proliferation^{43,46}.

4.2 *Irx3;Irx4* mutant mice as a mouse model of LVNC

It is widely accepted that the development of noncompaction occurs embryonically rather than postnatally²¹. The presence of morphological changes in *Irx4*KO and *Irx3;Irx4* double mutant embryonic hearts supports this theory. From the gross morphologies of normal and noncompact samples in published literature, it appears that the compaction process proceeds in a basal to apical manner^{65,66}. Noncompaction is mainly found in the apical regions as the mild phenotype of the *Irx4*KO hearts, while in the severe noncompaction phenotype of the *Irx3;Irx4*DKO mutants, prominent trabeculation appear from base to apex. These observations suggest that *Irx4*KO mice exhibit a premature arrest in the compaction process, which is hindered even earlier in *Irx3;Irx4*DKO mice. The phenotype worsens by birth to include striking, thickened trabeculation and abscesses in the ventricular wall with blood communication, all of which are classic characteristics of human LVNC²¹.

As well, noncompaction has been theorized to be due to hypertrabeculation, incomplete trabecular remodeling, or both. Indeed, there are human cases and mouse models supporting each or both phenotype²⁴, suggesting that these are two distinct pathways that result in a similar phenotype. The only difference between them is that in the first case, heart wall has normal thickness as normal amounts of trabecular remodeling occurred, and in the second case, the heart wall is thinner because of fewer trabeculae contributing to the wall formation. The failure to remodel the trabecular network in mice has been suggested to arise from altered proliferation patterns of cardiomyocytes³⁴.

This second scenario is consistent with the *Irx3;Irx4*DKO phenotype. As observed, by E14.5, the ventricular wall appears to be thinner in the DKO mice compared to the control, before a significantly different amount of trabeculation present is noted. *In situ* hybridization analysis at E13.5 also revealed an expanded noncompact region as indicated by the expression of the trabecular marker and a thinner compact region with the expression of the myocardial marker. These observations show that there is already a delay at the initiation of compaction, resulting in a thinner heart wall being formed. In the older animals characterized by OPT, *Irx3;Irx4*DKO mice also display regions of very thin wall structure, suggesting that the compaction process to form the heart wall never quite catches up to their littermate controls and the hearts retain a thinner and weaker ventricular wall.

To monitor the state of these diseased hearts, expression of diagnostic heart failure markers in the blood are commonly used as heart failure markers in humans and mice¹⁷. While the upregulation of the heart failure markers beta-MHC, ANP, and BNP are not as dramatic in the tissue itself, they are also frequently used in the literature for rodent models of cardiomyopathy. The range of published values for mice are between 1-fold and 20-fold increases in mRNA expression in mouse models of heart failure, depending on the severity and type of cardiomyopathy^{34,67-71}. In these studies, the upregulation of these genes have also been used to signify heart failure of the *Irx3;Irx4* mutants with comparable results of about 3- to 10-fold increases in their mRNA levels. However, Bruneau *et al.*⁵³ proposed that these same genes are up-regulated in the *Irx4*KO mice at 10 days of age not due to heart failure, but because *Irx4* controls the expression of these atrial genes. The main basis of their conclusion was that no cardiac phenotype was observed at 10 days. Nonetheless, this conclusion did not explain why these markers increased with age, which is what one would expect to see with on-going heart failure. With the novel *Irx4*KO phenotype observed in this study, it calls into question whether these genes are upregulated due to the noncompaction phenotype or mis-regulation by the absence of *Irx4*. To test this, an IRX4 ChIP-seq experiment will be informative to define the regulatory targets of IRX4 and to determine whether they include the expression of these heart failure marker genes.

When compared with published models of LVNC, *Irx3;Irx4*DKO mice exhibit a less severe phenotype. Most models tend to be embryonic lethal, dying between E12.5 and E16.5^{24,32,34}. For example, the FKBP12-deficient mutants, which displayed increased Bmp10 pathway activation,

mostly perished during embryogenesis and before weaning age, many of them succumbed within a few weeks due to a cardiac-related wasting syndrome⁴⁰. Most *Irx3;Irx4*DKO mutants also displayed a severe wasting syndrome, suggesting that this failure to thrive is a common characteristic of a failing heart in mice. We observed that *Irx3;Irx4*DKO mice exhibit a severe developmental delay, inability to gain weight, and the hallmarks of sick mice – ruffled fur and less movement. They have a partial postnatal lethality, dying around P21, likely when the heart cannot meet the demands of the rapidly growing body. In this regard, a novel and important aspect of this mouse model in comparison to other published mouse models of LVNC is that its later mortality is arguably a better model for human disease as human patients present with symptoms of LVNC throughout their life time, including adulthood²².

Compared to the morphology of human LVNC, the *Irx3;Irx4*DKO mouse phenotype is quite different from the classical presentation of LVNC, in which it is characterized by thin muscular projections near the apex of the heart, resembling fingerlike projections projecting straight into the ventricular chamber, and a thinner wall with abscesses around these projections. As Burke *et al.* described, however, the LVNC gross morphology can be further classified into three different groups²⁹. In accordance to this categorization, observations on the phenotype of *Irx3;Irx4*DKO mice using H&E staining as well as gross tissue structure matches very well with the polypoid form of LVNC, which is characterized by various muscular nodes in the left ventricular chamber resembling many papillary muscles. This alteration of muscle structure into many muscular bundles is not often found in human case reports, likely because it is harder to observe through echocardiography and only evident in retrospective studies during autopsies. The functional distinctions between these different types of LVNC have never been reported, although the rate of occurrence for this subtype appears to be quite high according to one small study of 14 cases of infantile-onset LVNC, with 6 positive for the polypoid phenotype²⁹.

The impact of this morphology on heart functions is not clear. It has never been characterized in humans and using mouse models, it is difficult to speculate due to other confounding heart defects present. In this study, we observed significantly different heart contractility of the double mutants at 5 weeks of age, which may be counter-intuitive considering the sicker mutant mice die before this age. However, the large variation in heart function of the mutants at 2 weeks of age is also seen in the human patients with LVNC. Specifically, young LVNC patients often showed instability of their echocardiographic measurements, where they can spontaneously

recover their systolic functions, then spontaneously worsen, until puberty, when their heart functions systematically decrease⁷².

Similarly in this regard, we found that *Irx3;Irx4*DKO mice show a much more consistent echocardiographic finding at 5 weeks of age, including mitral regurgitation. This was not unexpected, as it has been shown that altered papillary muscle support and weaker ventricular wall are sufficient to induce regurgitation in dogs¹³; both criteria are met in the *Irx3;Irx4*DKO hearts. In fact, a previous publication noted the link between LVNC and mitral regurgitation: there was an additional association with a lower amount of total papillary muscle area, suggesting that an abnormal papillary muscle anatomy may predispose to mitral regurgitation in LVNC⁷³. The *Irx3;Irx4*DKO model is therefore faithful to the human disease phenotype in its later onset of symptoms, providing an additional benefit to this postnatally viable disease model.

Furthermore, most trabeculation is present in the mid ventricular wall and apex, consistent with human patient data²⁸. Strikingly, these abnormal muscle projections can reach the thickness of the septum, and indeed, a muscular linkage between the septum and the apex was seen in almost all DKO hearts by echocardiography. While this specific phenotype is not known to be associated with LVNC, it is actually found in human patients of hypertrophy⁷⁴, suggesting that these abnormal muscle projections may be due to the *Irx4*KO hypertrophic cardiomyopathy phenotype. As well, the consistent linkage between septum and apex in the DKO mice by a muscular structure may be explained by the fact that trabeculation and interventricular septum are clonally related⁴. Interestingly, preliminary data showed that *Irx3;Irx4*DKO mice develop hypertrophy by 10 months of age correlating to the *Irx4*KO phenotype. While the timeline of developing hypertrophy is not changed in the mutant, it does provide support for a genetic basis for the occurrence of human LVNC with other cardiomyopathies²⁸.

4.3 *Irx3;Irx4* mutants have altered Bmp10 pathway expression which may contribute to noncompaction through continuous myocardial proliferation

Bmp10 is upregulated in both embryonic and postnatal mutant hearts. However, I found that Bmp10 pathway activity is only altered in the embryonic mutant hearts, suggesting that another postnatal regulatory network is likely involved. Interestingly, while many double mutants showed elevated Bmp10 expression, downstream activation of the Bmp10 pathway was only

observed in *Irx3^{+/-};Irx4^{-/-}* and *Irx3;Irx4*DKO hearts, which exhibit a noncompaction phenotype, as revealed by nuclear staining of pSMAD1/5/8. This implies that IRX4 has a regulatory function for the Bmp10 pathway, where a single dose of *Irx4* seems to be able to block downstream activation of the Bmp10 pathway. It will be interesting to explore how IRX4 exerts its action; whether it acts by controlling translation or secretion of Bmp10 or activation of the ALK1 receptor or events downstream of ALK1.

It is widely accepted in the literature that increased Bmp10 signaling results in increased proliferation, hindering the ability of the trabeculae to compact. In *Irx3;Irx4*DKO mice, there is a significant increased cell proliferation in the mid-basal and apical regions of the left ventricular wall. This supports the current theory in literature regarding proliferation and improper compaction.

This finding of the roles of IRX3 and IRX4 in cell proliferation is not unprecedented. The *Drosophila* Iroquois proteins have been found to regulate G1 to S transition through interactions with Cyclin E-containing protein complexes⁷⁵. IRX4 has been found to be a tumour suppressor gene in prostate cancer⁷⁶, though its role in cardiomyocyte proliferation has never been reported. In addition, *Irx* family members can potentially interact with other transcription factors NKX2.5 and TBX5 to regulate cardiomyocyte proliferation⁵⁰. Thus, their roles in cardiomyocyte proliferation deserve further investigations.

Our results here correlate well with published mouse models and provide additional links between different regulatory molecules of heart development. For example, IRX3, as a potential binding partner of the cardiac transcription factor NKX2.5⁵⁰, may contribute to the upregulation of *Bmp10* expression in *Nkx2.5*KO hearts. Furthermore, as NKX2.5 regulates *Irx4* expression in a DNA-binding dependent manner⁷⁷, the noncompaction phenotype of *Nkx2.5*KO mice can be attributed to reduced function of IRX3 and IRX4.

However, the relationship between proliferation and noncompaction is still unknown. Observations of mammalian heart morphological development show a thickening of the trabeculae at the base, whether due to cellular pathways or external forces acting upon them, gradually resulting in a collapse of the trabecular projections into the ventricular wall⁷⁸. Sedmera *et al.* found this process highly associated with the increase in luminal and ventricular volume¹¹, suggesting that external forces generated by these changes may contribute to the compaction

process. This would explain how proliferation would interrupt cardiac compaction. Normally the trabecular web collapse downward, much like a web being pulled taut, allowing the formation of a more discrete sheet structure. However, if the meshwork of trabeculae continues to grow into the chamber, then the external force will not be sufficient to resolve all the trabecular structures towards the compact wall, allowing for residual trabecular structures. Understandably, this hypothesis cannot explain those noncompaction models with decreased rates of cardiomyocyte proliferation⁷⁹, indicating that additional pathways and mechanisms are present in this complex developmental process.

4.4 Future Directions

Overall, *Irx3;Irx4*DKO mice provide a novel model for studying the basic heart compaction process and serve as a faithful model of the polypoid pattern of LVNC in humans. They exhibit both isolated morphological characteristics and functional defects associated with LVNC. However, while this study has demonstrated the overlapping roles of *Irx3* and *Irx4* in heart development, there are still many unresolved questions.

First, although I have investigated the role of the Bmp10 pathway in this study, the requirement of IRX3 and IRX4 in other signaling pathways and processes remains to be defined. Transcriptome analysis of *Irx3*KO, *Irx4*KO, and *Irx3;Irx4*DKO hearts should provide a global view of the pathways and genes that are altered by loss of *Irx3* and/or *Irx4*. I have begun the RNA-seq experiments by isolating mRNA from E14.5 heart samples of *Irx3*^{+/-};*Irx4*^{+/-}, *Irx3*KO, *Irx4*KO, and *Irx3;Irx4*DKO mice. This time-point was chosen because initiation of compaction occurs then, and changes in the transcriptome at this time-point are expected to reveal relevant events related to the noncompaction phenotype. The libraries have been sequenced, but the data analysis is not available yet for inclusion in this thesis. Hopefully, the RNA-seq results will shed light into potential signaling pathways associated with compaction and how alteration in proliferation may affect the compaction process. Comparison between the single KO and the DKO samples should unveil clues about the pathways that are exacerbated by the additional loss of *Irx3* in an *Irx4*KO background and the regulatory role of IRX4 in Bmp10 pathway activation, and help pinpoint the pathways involved in LVNC versus hypertrophic cardiomyopathy.

As IRX3 and IRX4 are known as transcription factors, it is also important to determine the transcriptional targets of IRX3 and IRX4. ChIP-seq analysis will offer an opportunity to

determine the direct targets of IRX3 and IRX4, and perhaps potential interactions with other transcription factors as well. Together with the transcriptome analysis, it should provide important insight about the role of these target genes in pathways involved in trabecular proliferation and compaction.

Additional experiments using cultures of isolated embryonic hearts may also provide confirmation of the direct role of Bmp10 in the *Irx3;Irx4* DKO model. Chen *et al.* had previously cultured embryonic hearts in Bmp10-conditioned media, promoting cardiomyocyte growth and ultimately rescuing the hypoplastic phenotype of *Bmp10* mutant hearts³⁴. We can employ these organ cultures to examine the effects of Bmp10-conditioned media and media containing a Bmp10 pathway inhibitor on our mutants. Their effects on cardiomyocyte proliferation and compaction could allow us to establish a causative relationship or not between Bmp10 pathway activity and the heart phenotypes of *Irx3;Irx4* mutant mice.

In closing, these studies have characterized the *Irx3;Irx4* mutant mice as a model of human LVNC. They can then be utilized for further studies on the compaction and myocardial muscle formation process, as well as identifying potential therapeutic targets for this congenital cardiomyopathy.

References

1. Kim KH, Rosen A, Bruneau BG, Hui CC, Backx PH. Iroquois homeodomain transcription factors in heart development and function. *Circ Res*. 2012;110(11):1513-1524.
2. Miquerol L, Kelly RG. Organogenesis of the vertebrate heart. *Wiley Interdiscip Rev Dev Biol*. 2013;2(1):17-29.
3. Sedmera D, Pexieder T, Vuillemin M, Thompson RP, Anderson RH. Developmental patterning of the myocardium. *Anat Rec*. 2000;258(4):319-337.
4. Meilhac SM, Kelly RG, Rocancourt D, Eloy-Trinquet S, Nicolas JF, Buckingham ME. A retrospective clonal analysis of the myocardium reveals two phases of clonal growth in the developing mouse heart. *Development*. 2003;130(16):3877-3889.
5. Zhang W, Chen H, Qu X, Chang CP, Shou W. Molecular mechanism of ventricular trabeculation/compaction and the pathogenesis of the left ventricular noncompaction cardiomyopathy (LVNC). *Am J Med Genet C Semin Med Genet*. 2013;163C(3):144-156.
6. Liu J, Bressan M, Hassel D, et al. A dual role for ErbB2 signaling in cardiac trabeculation. *Development*. 2010;137(22):3867-3875.
7. Chen H, Shi S, Acosta L, et al. BMP10 is essential for maintaining cardiac growth during murine cardiogenesis. *Development*. 2004;131(9):2219-2231.
8. Pasumarthi KB, Field LJ. Cardiomyocyte cell cycle regulation. *Circ Res*. 2002;90(10):1044-1054.

9. Kochilas LK, Li J, Jin F, Buck CA, Epstein JA. p57Kip2 expression is enhanced during mid-cardiac murine development and is restricted to trabecular myocardium. *Pediatr Res*. 1999;45(5 Pt 1):635-642.
10. Samsa LA, Yang B, Liu J. Embryonic cardiac chamber maturation: Trabeculation, conduction, and cardiomyocyte proliferation. *Am J Med Genet C Semin Med Genet*. 2013;163C(3):157-168.
11. Sedmera D, Pexieder T, Vuillemin M, Thompson RP, Anderson RH. Developmental patterning of the myocardium. *Anat Rec*. 2000;258(4):319-337.
12. Lamers WH, Wessels A, Verbeek FJ, et al. New findings concerning ventricular septation in the human heart. implications for maldevelopment. *Circulation*. 1992;86(4):1194-1205.
13. Oosthoek PW, Wenink AC, Wisse LJ, Gittenberger-de Groot AC. Development of the papillary muscles of the mitral valve: Morphogenetic background of parachute-like asymmetric mitral valves and other mitral valve anomalies. *J Thorac Cardiovasc Surg*. 1998;116(1):36-46.
14. Cheng TO. The vital role of papillary muscles in mitral and ventricular function: Echocardiographic insights. *Clin Cardiol*. 1997;20(5):506.
15. Wessels A, Sedmera D. Developmental anatomy of the heart: A tale of mice and man. *Physiol Genomics*. 2003;15(3):165-176.
16. Shemisa K, Li J, Tam M, Barcena J. Left ventricular noncompaction cardiomyopathy. *Cardiovasc Diagn Ther*. 2013;3(3):170-175.
17. Sato Y, Fujiwara H, Takatsu Y. Biochemical markers in heart failure. *J Cardiol*. 2012;59(1):1-7.

18. Freedom RM, Yoo SJ, Perrin D, Taylor G, Petersen S, Anderson RH. The morphological spectrum of ventricular noncompaction. *Cardiol Young*. 2005;15(4):345-364.
19. Maron BJ, Towbin JA, Thiene G, et al. Contemporary definitions and classification of the cardiomyopathies: An american heart association scientific statement from the council on clinical cardiology, heart failure and transplantation committee; quality of care and outcomes research and functional genomics and translational biology interdisciplinary working groups; and council on epidemiology and prevention. *Circulation*. 2006;113(14):1807-1816.
20. Breckenridge RA, Anderson RH, Elliott PM. Isolated left ventricular noncompaction: The case for abnormal myocardial development. *Cardiol Young*. 2007;17(2):124-129.
21. Ichida F. Left ventricular noncompaction. *Circ J*. 2009;73(1):19-26.
22. Hoedemaekers YM, Caliskan K, Michels M, et al. The importance of genetic counseling, DNA diagnostics, and cardiologic family screening in left ventricular noncompaction cardiomyopathy. *Circ Cardiovasc Genet*. 2010;3(3):232-239.
23. Daubeney PE, Nugent AW, Chondros P, et al. Clinical features and outcomes of childhood dilated cardiomyopathy: Results from a national population-based study. *Circulation*. 2006;114(24):2671-2678.
24. Oechslin E, Jenni R. Left ventricular noncompaction revisited: A distinct phenotype with genetic heterogeneity? *Eur Heart J*. 2011;32(12):1446-1456.
25. Grant RT. An unusual anomaly of the coronary vessels in the malformed heart of a child. *Heart*. 1926;13:273-283.

26. Arunamata A, Punni R, Cuneo B, Bharati S, Silverman NH. Echocardiographic diagnosis and prognosis of fetal left ventricular noncompaction. *J Am Soc Echocardiogr*. 2012;25(1):112-120.
27. Bennett CE, Freudenberg R. The current approach to diagnosis and management of left ventricular noncompaction cardiomyopathy: Review of the literature. *Cardiol Res Pract*. 2016;2016:5172308.
28. Jenni R, Oechslin E, Schneider J, Attenhofer Jost C, Kaufmann PA. Echocardiographic and pathoanatomical characteristics of isolated left ventricular noncompaction: A step towards classification as a distinct cardiomyopathy. *Heart*. 2001;86(6):666-671.
29. Burke A, Mont E, Kutys R, Virmani R. Left ventricular noncompaction: A pathological study of 14 cases. *Hum Pathol*. 2005;36(4):403-411.
30. Yang J, Bucker S, Jungblut B, et al. Inhibition of Notch2 by numb/numbl-like controls myocardial compaction in the heart. *Cardiovasc Res*. 2012;96(2):276-285.
31. Pashmforoush M, Lu JT, Chen H, et al. Nkx2-5 pathways and congenital heart disease; loss of ventricular myocyte lineage specification leads to progressive cardiomyopathy and complete heart block. *Cell*. 2004;117(3):373-386.
32. Chen H, Zhang W, Sun X, et al. Fkbp1a controls ventricular myocardium trabeculation and compaction by regulating endocardial Notch1 activity. *Development*. 2013;140(9):1946-1957.
33. Probst S, Oechslin E, Schuler P, et al. Sarcomere gene mutations in isolated left ventricular noncompaction cardiomyopathy do not predict clinical phenotype. *Circ Cardiovasc Genet*. 2011;4(4):367-374.

34. Chen H, Shi S, Acosta L, et al. BMP10 is essential for maintaining cardiac growth during murine cardiogenesis. *Development*. 2004;131(9):2219-2231.
35. Chen H, Zhang W, Li D, Cordes TM, Mark Payne R, Shou W. Analysis of ventricular hypertrabeculation and noncompaction using genetically engineered mouse models. *Pediatr Cardiol*. 2009;30(5):626-634.
36. Grego-Bessa J, Luna-Zurita L, del Monte G, et al. Notch signaling is essential for ventricular chamber development. *Dev Cell*. 2007;12(3):415-429.
37. Lai D, Liu X, Forrai A, et al. Neuregulin 1 sustains the gene regulatory network in both trabecular and nontrabecular myocardium. *Circ Res*. 2010;107(6):715-727.
38. Stankunas K, Hang CT, Tsun ZY, et al. Endocardial Brg1 represses ADAMTS1 to maintain the microenvironment for myocardial morphogenesis. *Dev Cell*. 2008;14(2):298-311.
39. Luxan G, Casanova JC, Martinez-Poveda B, et al. Mutations in the NOTCH pathway regulator MIB1 cause left ventricular noncompaction cardiomyopathy. *Nat Med*. 2013;19(2):193-201.
40. Shou W, Aghdasi B, Armstrong DL, et al. Cardiac defects and altered ryanodine receptor function in mice lacking FKBP12. *Nature*. 1998;391(6666):489-492.
41. Wang T, Li BY, Danielson PD, et al. The immunophilin FKBP12 functions as a common inhibitor of the TGF beta family type I receptors. *Cell*. 1996;86(3):435-444.
42. Watanabe Y, Kokubo H, Miyagawa-Tomita S, et al. Activation of Notch1 signaling in cardiogenic mesoderm induces abnormal heart morphogenesis in mouse. *Development*. 2006;133(9):1625-1634.

43. Del Monte G, Grego-Bessa J, Gonzalez-Rajal A, Bolos V, De La Pompa JL. Monitoring Notch1 activity in development: Evidence for a feedback regulatory loop. *Dev Dyn*. 2007;236(9):2594-2614.
44. Suri C, Jones PF, Patan S, et al. Requisite role of angiopoietin-1, a ligand for the TIE2 receptor, during embryonic angiogenesis. *Cell*. 1996;87(7):1171-1180.
45. Lavine KJ, Yu K, White AC, et al. Endocardial and epicardial derived FGF signals regulate myocardial proliferation and differentiation in vivo. *Dev Cell*. 2005;8(1):85-95.
46. Kang JO, Sucov HM. Convergent proliferative response and divergent morphogenic pathways induced by epicardial and endocardial signaling in fetal heart development. *Mech Dev*. 2005;122(1):57-65.
47. Christoffels VM, Keijser AG, Houweling AC, Clout DE, Moorman AF. Patterning the embryonic heart: Identification of five mouse iroquois homeobox genes in the developing heart. *Dev Biol*. 2000;224(2):263-274.
48. Zhang SS, Kim KH, Rosen A, et al. Iroquois homeobox gene 3 establishes fast conduction in the cardiac his-purkinje network. *Proc Natl Acad Sci U S A*. 2011;108(33):13576-13581.
49. Zhang W, Chen H, Wang Y, et al. Tbx20 transcription factor is a downstream mediator for bone morphogenetic protein-10 in regulating cardiac ventricular wall development and function. *J Biol Chem*. 2011;286(42):36820-36829.
50. Kim KH, Rosen A, Hussein SM, et al. Irx3 is required for postnatal maturation of the mouse ventricular conduction system. *Sci Rep*. 2016;6:19197.

51. Koizumi A, Sasano T, Kimura W, et al. Genetic defects in a his-purkinje system transcription factor, IRX3, cause lethal cardiac arrhythmias. *Eur Heart J*. 2016;37(18):1469-1475.
52. He W, Jia Y, Takimoto K. Interaction between transcription factors iroquois proteins 4 and 5 controls cardiac potassium channel Kv4.2 gene transcription. *Cardiovasc Res*. 2009;81(1):64-71.
53. Bruneau BG, Bao ZZ, Fatkin D, et al. Cardiomyopathy in Irx4-deficient mice is preceded by abnormal ventricular gene expression. *Mol Cell Biol*. 2001;21(5):1730-1736.
54. Cheng Z, Wang J, Su D, et al. Two novel mutations of the IRX4 gene in patients with congenital heart disease. *Hum Genet*. 2011;130(5):657-662.
55. Gaborit N, Sakuma R, Wylie JN, et al. Cooperative and antagonistic roles for Irx3 and Irx5 in cardiac morphogenesis and postnatal physiology. *Development*. 2012;139(21):4007-4019.
56. Costantini DL, Arruda EP, Agarwal P, et al. The homeodomain transcription factor Irx5 establishes the mouse cardiac ventricular repolarization gradient. *Cell*. 2005;123(2):347-358.
57. Thomas L, Foster E, Schiller NB. Peak mitral inflow velocity predicts mitral regurgitation severity. *J Am Coll Cardiol*. 1998;31(1):174-179.
58. Chakraborty S, Yutzey KE. Tbx20 regulation of cardiac cell proliferation and lineage specialization during embryonic and fetal development in vivo. *Dev Biol*. 2012;363(1):234-246.
59. Chang Z, Zhang Q, Feng Q, et al. Deletion of Akt1 causes heart defects and abnormal cardiomyocyte proliferation. *Dev Biol*. 2010;347(2):384-391.

60. Misra C, Chang SW, Basu M, Huang N, Garg V. Disruption of myocardial Gata4 and Tbx5 results in defects in cardiomyocyte proliferation and atrioventricular septation. *Hum Mol Genet.* 2014;23(19):5025-5035.
61. Mo R, Freer AM, Zinyk DL, et al. Specific and redundant functions of Gli2 and Gli3 zinc finger genes in skeletal patterning and development. *Development.* 1997;124(1):113-123.
62. Hui CC, Joyner AL. A mouse model of greig cephalopolysyndactyly syndrome: The extra-toesJ mutation contains an intragenic deletion of the Gli3 gene. *Nat Genet.* 1993;3(3):241-246.
63. Wong MD, Dazai J, Walls JR, Gale NW, Henkelman RM. Design and implementation of a custom built optical projection tomography system. *PLoS One.* 2013;8(9):e73491.
64. Sharpe J, Ahlgren U, Perry P, et al. Optical projection tomography as a tool for 3D microscopy and gene expression studies. *Science.* 2002;296(5567):541-545.
65. Ikeda U, Minamisawa M, Koyama J. Isolated left ventricular noncompaction cardiomyopathy in adults. *J Cardiol.* 2015;65(2):91-97.
66. Shemisa K, Li J, Tam M, Barcena J. Left ventricular noncompaction cardiomyopathy. *Cardiovasc Diagn Ther.* 2013;3(3):170-175.
67. Arber S, Hunter JJ, Ross J, Jr, et al. MLP-deficient mice exhibit a disruption of cardiac cytoarchitectural organization, dilated cardiomyopathy, and heart failure. *Cell.* 1997;88(3):393-403.
68. Fan G, Jiang YP, Lu Z, et al. A transgenic mouse model of heart failure using inducible galpha q. *J Biol Chem.* 2005;280(48):40337-40346.

69. Tsoutsman T, Kelly M, Ng DC, et al. Severe heart failure and early mortality in a double-mutation mouse model of familial hypertrophic cardiomyopathy. *Circulation*. 2008;117(14):1820-1831.
70. Chien KR, Knowlton KU, Zhu H, Chien S. Regulation of cardiac gene expression during myocardial growth and hypertrophy: Molecular studies of an adaptive physiologic response. *FASEB J*. 1991;5(15):3037-3046.
71. Chiu HC, Kovacs A, Ford DA, et al. A novel mouse model of lipotoxic cardiomyopathy. *J Clin Invest*. 2001;107(7):813-822.
72. Pignatelli RH, McMahon CJ, Dreyer WJ, et al. Clinical characterization of left ventricular noncompaction in children: A relatively common form of cardiomyopathy. *Circulation*. 2003;108(21):2672-2678.
73. Stacey RB, Haag J, Hall ME, et al. Mitral regurgitation in left ventricular noncompaction cardiomyopathy assessed by cardiac MRI. *J Heart Valve Dis*. 2014;23(5):591-597.
74. Sung KT, Yun CH, Hou CJ, Hung CL. Solitary accessory and papillary muscle hypertrophy manifested as dynamic mid-wall obstruction and symptomatic heart failure: Diagnostic feasibility by multi-modality imaging. *BMC Cardiovasc Disord*. 2014;14:34-2261-14-34.
75. Barrios N, Gonzalez-Perez E, Hernandez R, Campuzano S. The homeodomain iroquois proteins control cell cycle progression and regulate the size of developmental fields. *PLoS Genet*. 2015;11(8):e1005463.

76. Nguyen HH, Takata R, Akamatsu S, et al. IRX4 at 5p15 suppresses prostate cancer growth through the interaction with vitamin D receptor, conferring prostate cancer susceptibility. *Hum Mol Genet.* 2012;21(9):2076-2085.
77. Bruneau BG, Bao ZZ, Tanaka M, et al. Cardiac expression of the ventricle-specific homeobox gene *Irx4* is modulated by *Nkx2-5* and *dHand*. *Dev Biol.* 2000;217(2):266-277.
78. Samsa LA, Yang B, Liu J. Embryonic cardiac chamber maturation: Trabeculation, conduction, and cardiomyocyte proliferation. *Am J Med Genet C Semin Med Genet.* 2013;163C(3):157-168.
79. Kosaka Y, Cieslik KA, Li L, et al. 14-3-3epsilon plays a role in cardiac ventricular compaction by regulating the cardiomyocyte cell cycle. *Mol Cell Biol.* 2012;32(24):5089-5102.